Pressure-Temperature Operating Curves for Nine Mile Point Unit 1

May, 1998

© Copyright MPM Technologies, Inc. 1998
All Rights Reserved

MPM ....SERVING CLIENT NEEDS THROUGH ADVANCED TECHNOLOGY

Report No. MPM-59838

9807240396 980619
PDR ADOCK 05000220
P PDR

Report No. MPM-59838

Final Report

entitled

Pressure-Temperature Operating Curves for Nine Mile Point Unit 1

Prepared for:

Niagara Mohawk Power Corporation
Nine Mile Point Unit 1
Lake Road
Lycoming, NY 13093

by:

Dr. Michael P. Manahan, Sr.
MPM Technologies, Inc.
2161 Sandy Drive
State College, PA 16803-2283

May, 1998

© Copyright MPM Technologies, Inc. 1998
All Rights Reserved

Contents

Executive Summary ii

1.0 Introduction 1
- 1.1 Chapter 1 Reference 1

2.0 Calculative Procedure 2
- 2.1 RT_{NDT} Shift Determination 3
- 2.2 Pressure-Temperature (P-T) Curve Development 3
  - 2.2.1 Limiting Stress Intensity Factor Conditions 5
  - 2.2.2 Thermal Analysis 5
  - 2.2.3 Stress Intensity Indices 6
  - 2.2.4 Allowable Coolant Temperature and Pressure 6
- 2.3 Chapter 2 References 7

3.0 Neutron Flux Calculation 8
- 3.1 Introduction 8
- 3.2 Neutron Transport Model 8
- 3.3 Neutron Transport Results 10
- 3.4 Analysis of Dosimetry Data 12
  - 3.4.1 Capsule B Dosimetry Analysis 12
  - 3.4.2 Comparison of 210 and 300 Degree Capsules 13
  - 3.4.3 Capsule Fluence Uncertainty Analysis 14
- 3.5 Vessel Fluence Evaluation and Projection 15
  - 3.5.1 R-Z Transport Results 15
  - 3.5.2 In-vessel Peak Fluence Calculations 15
  - 3.5.3 Vessel Fluence Uncertainty Analysis 16
- 3.6 Chapter 3 References 16

4.0 Pressure-Temperature Curve Analysis 30
- 4.1 Neutron Fluence Determination 30
- 4.2 Surveillance Data Assessment 30
- 4.3 ART For Limiting RPV Material 31
- 4.4 Thermal Transient Analysis 32
- 4.5 Minimum Temperature for Critical Core Operation 33
- 4.6 Summary of Plant Parameters 33
- 4.7 P-T Curves 34
- 4.8 Chapter 4 References 34

5.0 Summary 55

6.0 Nomenclature 56

Executive Summary

Reactor pressure vessel (RPV) materials undergo a transition in fracture behavior from brittle to ductile as the test temperature of the material is increased. Charpy V-notch tests are conducted in the nuclear industry to monitor changes in the fracture behavior during irradiation. Neutron irradiation to fluences above ~5 x 10^{16} n/cm^2 causes an upward shift in the Charpy curve and in the ductile-to-brittle transition temperature (DBTT). In order to ensure safe operation of a nuclear power plant during heatup, cooldown, and leakage/hydrotest conditions, it is necessary to conservatively calculate allowable stress loadings for the ferritic RPV materials. These allowable loadings can be conveniently presented as a plot of measured coolant pressure versus measured coolant temperature (P-T curves). Appendix G to 10CFR50 and Appendix G to Section III of the American Society of Mechanical Engineers (ASME) Boiler and Pressure Vessel Code present a procedure for obtaining the allowable loadings for ferritic pressure-retaining materials in Class 1 components. Neutron damage within the RPV during plant operation is accounted for in the allowable pressure loading by calculating an adjusted reference temperature (ART). Regulatory Guide 1.99, Revision 2 (RG1.99(2)) defines the ART as the sum of the initial unirradiated nil-ductility reference temperature (RT_{NDT}) plus the RT_{NDT} irradiation induced shift (ΔRT_{NDT}) plus a margin term. Within the nuclear industry, the ΔRT_{NDT} is determined from the Charpy transition curve shift indexed at 30 ft-lbs of absorbed energy.

Previous P-T limits for Nine Mile Point Unit 1 (NMP-1) were calculated up to 18 effective full power years (EFPY) [1-1]. At the time the previous P-T limits were calculated, three plate surveillance data points were available. In March, 1997, the 210 degree surveillance capsule (Capsule B) was withdrawn and tested [3-13]. As a result of this work, a fourth plate surveillance data point has become available. These data have been used to re-evaluate the ART values for the vessel beltline materials and to update and extend the operating pressure-temperature (P-T) limit curves using projected vessel fluence levels. A Technical Specification Amendment Application has been prepared to extend the valid operating period to 28 EFPY. This report documents the calculations and analyses performed in support of the Technical Specification Amendment.

1.0 Introduction

To ensure safe operation of a nuclear power plant during heatup, cooldown, and leakage/ hydrostatic testing conditions, it is necessary to conservatively calculate allowable stress loadings for the ferritic reactor pressure vessel (RPV) materials. These allowable loadings are presented as a plot of measured coolant pressure versus measured coolant temperature (P-T curves). The P-T curves currently in use at Nine Mile Point Unit 1 (NMP-1) are valid for up to 18 EFPY [1-1] which is expected to be reached in December, 1998. Therefore, a Technical Specification Amendment Application has been prepared to extend the valid operating period to 28 EFPY. In addition to the leak/hydro test curve for 28 EFPY, leak/hydro test curves have been prepared for exposures up to 20 EFPY and up to 24 EFPY to shorten outage time for startups conducted prior to these exposures.

This report documents the methods used to obtain the revised P-T curves. Section 2.0 presents the methodology used for P-T curve calculation. Section 3.0 presents the results of neutron transport calculations which were preformed to more accurately determine the Capsule B exposure and to calculate the peak flux at the vessel ID surface. Section 4.0 presents the plant data used in the calculations and the resulting P-T curves. Section 5.0 briefly summarizes key features of the new P-T curves.

1.1 Chapter 1 Reference

[1-1] Manahan, M. P., "Pressure-Temperature Operating Curves for Nine Mile Point Unit 1", Report Number NMEL-90002, January, 1991.

2.0 Calculative Procedure

The regulations governing the calculation of P-T limits for the reactor coolant pressure boundary are found in the Code of Federal Regulations (CFR), the ASME Boiler and Pressure Vessel Code, and Regulatory Guides. As stated in Reference [2-1], the following are the regulations requiring P-T limits:

> "Paragraph 50.55a of 10 CFR Part 50, "Codes and Standards," requires that structures, systems, and components be designed, fabricated, erected, constructed, tested, and inspected to quality standards commensurate with the importance of the safety function to be performed. In addition, General Design Criterion 1 of Appendix A of 10 CFR Part 50, "Quality Standards and Records," requires that the codes and standards used to assure quality products in keeping with the safety function be identified and evaluated to determine their adequacy.
>
> General Design Criterion 14 of Appendix A of 10 CFR Part 50, "Reactor Coolant Pressure Boundary," requires that the reactor coolant pressure boundary be designed, fabricated, erected, and tested in order to have an extremely low probability of abnormal leakage, of rapid failure, and of gross rupture. Likewise, General Design Criterion 31, "Fracture Prevention of Reactor Coolant Pressure Boundary," requires, in part, that the reactor coolant pressure boundary be designed with sufficient margin to assure that when stressed under operating, maintenance and testing, the boundary behaves in a nonbrittle manner and the probability of rapidly propagating fracture is minimized. Further, in order to assess the structural integrity of the reactor vessel, General Design Criterion 32, "Inspection of Reactor Coolant Pressure Boundary," requires, in part, an appropriate materials surveillance program for the reactor vessel beltline region."

The fracture toughness requirements for the reactor pressure vessel (RPV) for testing and operational conditions are specified in Section IV of 10CFR50, Appendix G. This appendix requires implementation of the acceptance and performance criteria of Appendix G to Section III of the ASME code. The basis for the technical requirements of the ASME code are discussed in Reference [2-2]. Appendix G to 10CFR50 requires that the effects of neutron irradiation on the RT_{NDT} of the beltline materials must be included in the P-T curve calculations. The guidance provided in the latest revision to Regulatory Guide 1.99 may be used for this purpose.

The calculations performed for NMP-1 fully satisfy the requirements of 10CFR50 Appendix G and Appendix G to Section III of the ASME Code. The two key models used in the calculation, the ΔRT_{NDT} model and the P-T limit model, are briefly summarized in the report sections which follow.

2.1 RT_{NDT} Shift Determination

Neutron damage within the RPV during plant operation is accounted for in the allowable pressure loading by calculating an adjusted reference temperature (ART). Regulatory Guide 1.99, Revision 2 [2-3] (RG1.99(2)) defines the ART as the sum of the initial unirradiated nil-ductility reference temperature (RT_{NDT}) plus the RT_{NDT} irradiation induced shift (ΔRT_{NDT}) plus a margin term. Within the nuclear industry, the ΔRT_{NDT} is determined from the Charpy transition curve shift indexed at 30 ft-lbs of absorbed energy. The ART for the vessel beltline region enters the P-T calculations directly via the ASME reference stress intensity factor relation (K_{IR}). Therefore, it is necessary to provide reasonable and conservative estimates of the shift in nil-ductility reference temperature for the period of time over which the P-T curves will be used. The ΔRT_{NDT} for NMP-1 was calculated using the guidance given in Revision 2 to Regulatory Guide 1.99 [2-3]. The functional form for the RG1.99(2) model is as follows:

$$\Delta RT_{NDT} = (CF)\, f^{(0.28-0.1 \log f)}$$

where,

CF	=	chemistry factor: based on Cu and Ni content in the RG1.99(2) Tables, or on the fitted surveillance data under Regulatory Position 2.1
f	=	fast fluence (E > 1 MeV) in units of 10^{19} n/cm^2

The beltline material with the limiting ART has been determined using the RG1.99 (2) CF for the non-surveillance beltline materials. Following the guidance given in RG1.99 (2) and [2-4], the CF for the G-8-1 surveillance plate was calculated using the Tables and this CF was compared to the CF determined from the surveillance data. Since the surveillance CF is more conservative than the Table CF for NMP-1, the surveillance CF has been used for this material. The result of this analysis was to show that plate G-307-4/5 has the limiting ART. Further details are provided in Section 4.0.

2.2 Pressure-Temperature (P-T) Curve Development

Appendix G [2-5] of the ASME Boiler and Pressure Vessel Code presents a procedure for obtaining the allowable loadings for ferritic pressure-retaining materials in Class 1 components. This procedure is based on the principles of linear elastic fracture mechanics. The calculative method used to determine the NMP-1 P-T curves satisfies the requirements of the ASME procedure.

The model uses the following governing relation for calculation of heatup and cooldown curves for the reactor vessel:

$$K_{IR} > 2\, K_{IM} + K_{IT} \qquad (2\text{-}1)$$

The Code requires that a semi-elliptical, axially oriented 1/4 thickness (T) reference flaw be postulated at the inside (1/4 T) and the outside (3/4 T) surfaces of the vessel to calculate the applied stress intensity factors. As a result of this assumption, equation (2-1) can be re-written as follows:

$$K_{IR} > 2\, M_m\, \sigma + M_t\ \Delta T_{max} \qquad (2\text{-}2)$$

where,

σ	=	vessel hoop stress (ksi)
K_{IT}	=	stress intensity factor produced by a radial thermal gradient across the wall (ksi$\sqrt{\text{in}}$)
K_{IM}	=	stress intensity factor corresponding to membrane tension (ksi$\sqrt{\text{in}}$)
K_{IR}	=	reference stress intensity factor (ksi$\sqrt{\text{in}}$)
M_m	=	stress intensity index for membrane stress ($\sqrt{\text{in}}$)
M_t	=	stress intensity index for thermal stress (ksi$\sqrt{\text{in}}$/F)
ΔT_{max}	=	temperature difference through the vessel wall during heatup and cooldown (F).

The reference stress intensity factor, K_{IR}, is calculated using the relationship given in Paragraph G-2110 of Appendix G which is:

$$K_{IR} = 26.777 + 1.223 \exp\left(0.0145\,(T - RT_{NDT} + 160)\right) \qquad (2\text{-}3)$$

where,

T	=	vessel metal temperature (F)
RT_{NDT}	=	nil-ductility reference temperature of the limiting RPV material.

This analytical approximation for K_{IR} is based on the lower bound of static, dynamic, and crack-arrest critical stress intensity values measured as a function of temperature on specimens of SA533B and SA508 steel.

For leak/hydro test, the Code allows reduction of the membrane stress intensity safety factor from 2 to 1.5. The thermal stress intensity factor is eliminated by ensuring the thermal gradient is negligible prior to pressurization for testing. The leak/hydro equation for the case where the core is not critical is therefore given by:

$$K_{IR} > 1.5\, K_{IM} \qquad (2\text{-}4)$$

2.2.1 Limiting Stress Intensity Factor Conditions

Heatup

For the case of vessel heatup, two conditions are analyzed: the stresses at the 1/4 thickness (1/4 T) location; and the 3/4 thickness (3/4 T) location. At the 1/4 T position, the thermal stresses on heatup are compressive and the membrane stresses are tensile. Therefore, the most highly stressed condition is when the thermal stresses equal zero at an isothermal condition. Thus, the hypothetical case of an isothermal heatup, 0 F/hr, is considered and applied to the heatup curves for conservatism.

For a postulated outside surface flaw with a crack tip at the 3/4 T position, the thermal stresses and membrane stresses are tensile and therefore additive. As a result, the maximum thermal stresses for a particular heating rate are superimposed on the pressure stresses in order to develop conservative heatup curves. Therefore, at the 3/4 T position, a total of 6 cases are considered: 0 F/hr; 20 F/hr; 40 F/hr; 60 F/hr; 80 F/hr; and 100 F/hr. The most limiting of the 1/4 T and 3/4 T (i.e., inside or outside) conditions is used to form the heatup curve.

Cooldown

For the case of cooldown, the pressure calculations need only be performed for an inside surface flaw at the 1/4 T location since the membrane and thermal stresses are tensile and additive. The 3/4 T location (i.e., outside surface) will always be stressed to a lesser or equal value and thus need not be considered. Therefore, at the 1/4 T position, a total of six cases are considered for cooldown: 0 F/hr; 20 F/hr; 40 F/hr; 60 F/hr; 80 F/hr; and 100 F/hr.

Leak/Hydro Test

For leakage and hydrostatic testing, the ASME rules allow elimination of the thermal gradient term since it is assumed that the vessel will be thermally equilibrated at the time the test pressure is applied. Therefore, the limiting loading condition is the membrane stress at the 1/4 T (i.e., inside surface) position.

2.2.2 Thermal Analysis

The temperature gradients in the pressure vessel wall at several heating and cooling rates are determined by performing transient thermal analyses using the Livermore multi-dimensional transient temperature distribution code (TRUMP) [2-6] computer program. The transient conditions result in a temperature difference through the vessel wall and a temperature difference from the inner diameter (ID) surface to the 1/4 T and 3/4 T positions. Thermal conductivity data for American Society for Testing and Materials (ASTM) A533 Grade B low alloy steel is taken from Appendix I of Section III of the ASME Code [2-7] and specific heat data are obtained from the thermophysical properties of matter data series (TRPC) Data Series [2-8].

2.2.3 Stress Intensity Indices

The ASME stress intensity indices (M_m and M_t) are calculated using the procedures of Appendix G of the ASME Code [2-5]. Use of the thermal stress intensity factor, M_t, provided in Appendix G of the ASME Code is appropriate provided the temperature change starts at a steady state condition, has a rate of change of less than 100F/hr, and the shape of the thermal gradient is approximately as given in Figure G-2214-3 of the ASME Code. The former conditions were satisfied as described above and the latter condition was satisfied by comparison of the thermal transient output with the ASME thermal gradient profile.

2.2.4 Allowable Coolant Temperature and Pressure

It is essential that the pressure and temperature variables plotted be consistent with the readings taken in the control room during operation. Based on discussions with plant personnel, the most useful plot is reactor vessel top dome pressure versus beltline downcomer water temperature. During plant operation, the temperature is measured in the recirculation pump suction line. This temperature is conservative as compared with the beltline downcomer water temperature since the actual reactor beltline temperature will be higher due to gamma heating effects and coolant frictional flow heating. Also, the instrument error must be included in a conservative manner. Therefore, we have:

$$T_C = T_{MEASURED} - T_{ERROR} \tag{2-5}$$

where,

T_C	=	downcomer coolant temperature
$T_{MEASURED}$	=	coolant temperature measured in the recirculation pump suction line
T_{ERROR}	=	temperature measurement instrument error

The pressure, since it is measured in the vessel steam region, must be corrected to the pressure at the bottom of the vessel. This can be done by adding the head of water from the top of the vessel to the bottom of the downcomer. Thus the pressure drop is conservatively estimated so that the pressure can be measured anywhere in the steam region of the vessel. Also, the pressure measurement error must be included in a conservative manner:

$$P_{RV} = P_{MEASURED} + P_{HEAD} + P_{ERROR} \tag{2-6}$$

where,

P_{RV}	=	core pressure at the bottom of the beltline region.
$P_{MEASURED}$	=	the core pressure measured in the top dome.
P_{HEAD}	=	head of from the top of the vessel to the bottom of the downcomer.
P_{ERROR}	=	pressure measurement instrument error.

2.3 Chapter 2 References

[2-1] Standard Review Plan, 5.3.2 Pressure-Temperature Limits, NUREG-0800, Revision 1 July 1981.

[2-2] Welding Research Council (WRC) Bulletin 175, "PVRC Recommendation on Toughness Requirements for Ferritic Materials," August 1972.

[2-3] U.S. NRC Regulatory Guide 1.99, "Radiation Embrittlement of Reactor Vessel Materials," Revision 2, May 1988.

[2-4] NRC/Industry Workshop on RPV Integrity Issues, "Generic Letter 92-01 and RPV Integrity Assessment", February 12, 1998

[2-5] ASME Boiler and Pressure Vessel Code, Section III, Appendix G for Nuclear Power Plant Components, Division 1, "Protection Against Nonductile Failure,".

[2-6] Edwards, A. L., "TRUMP: A Computer Program for Transient and Steady-State Temperature Distributions in Multidimensional Systems," Lawrence Radiation Laboratory, Livermore, Report UCRL-14754, Revision 2 (1968).

[2-7] ASME Boiler and Pressure Vessel Code, Section III, Appendix I.

[2-8] Touloukian, Y. S., Power, R. W., Ho, C. Y., and Klemens, P. G, The TPRC Data Series, Thermalphysical Properties of Matter, Volume 1, Thermal Conductivity, Metallic Elements and Alloys, Purdue Research Foundation, June 1972.

3.0 Neutron Flux Calculation

3.1 Introduction

The neutron exposure of surveillance capsule material specimens is determined by a combination of calculation and measurement. To monitor the exposure, radiometric monitors such as iron, nickel, and copper dosimeter wires are placed in the capsule and analyzed at the time of capsule removal to provide a measurement of the integrated fluence rate. To interpret the measurements, a calculated neutron spectrum at the capsule location is necessary, together with the operating power history of the reactor. The calculated neutron spectrum is determined by a neutron transport calculation.

The neutron transport calculation also evaluates the fluence at all points of interest in the reactor geometry, so that property changes in the vessel can be related to the capsule measurements. The calculation determines the distribution of neutrons of all energies from their source from fission in the core region to their eventual absorption or leakage from the system. The calculation uses a model of the reactor geometry that includes the significant structures and geometrical details as necessary to define the neutron environment at locations of interest.

3.2 Neutron Transport Model

The transport calculations for NMP-1 were carried out in R-θ and R-Z geometry using the DORT two-dimensional discrete ordinates code [3-1] and the BUGLE-96 cross-section library [3-2]. The DORT code is an update of the DOT code which has been in use for this type of problem for many years. The BUGLE-96 library is a 47 energy group ENDF/B-VI based data set produced specifically for light water reactor applications (an update of the earlier SAILOR library). This library contains cross-sections collapsed using a BWR core spectrum which were used for the core region. Outside the core region, cross sections collapsed using PWR downcomer and PWR vessel spectra were used. The difference between BWR and PWR collapsing in these regions is not significant. In these analyses, anisotropic scattering was treated with a P_3 expansion of the scattering cross-sections, and the angular discretization was modeled with an S_8 order of angular quadrature. These procedures are in accordance with ASTM Standard E-482 [3-3].

The R-θ layout is shown in Figure 3-1. In this figure all structures outside the core were modeled with a cylindrical symmetry except for the inclusion of a surveillance capsule centered at 30°. The R-θ model included 142 mesh points in the radial direction covering the range from the center of the core to the outside of the reactor vessel. Regions outside the reactor vessel were not included in the model. In the azimuthal direction, 33 mesh points were used to model a single octant of the reactor. Inspection of the fuel loading patterns indicated that only minor deviations from an octant symmetry were present. In the discussion below, all angles are referred to in the first octant (i.e relative to the nearest cardinal axis) and thus the capsule at 210°

(Capsule B) is centered at 30°. The mesh spacing was chosen to limit the changes in flux between mesh points to values significantly less than a factor of 2. For example, typical fast flux changes between radial mesh points in the vessel were about 20%.

The capsule was modeled with 3 mesh points in the radial direction and 3 mesh points in the azimuthal direction. Since the dosimetry was located at the center of the capsule (both radially and azimuthally, the capsule center mesh point best represents the neutron flux spectrum for the dosimetry analysis. The GE capsules are arranged with the dosimetry wires on the top of the Charpy specimens (the capsules are one Charpy bar thick). The three packets are stacked adjacent to one another which results in the dosimeters being axially separated by ~ 2 inches. Therefore, since the axial variation over this distance is small, the core midplane calculations are applicable for interpretation of the dosimetry data.

The core region used a homogenized material distribution which includes the fuel, fuel cladding, and the water. The water region in the fuel contains both liquid water and steam. The fraction occupied by steam is known as the void fraction and varies by assembly and axial position within the fuel. Values of void fraction for Cycle 12 were supplied by Niagara Mohawk for each of the outer assemblies at axial midplane [3-4]. Inspection of these values indicated that significant variation in the void fraction occurred, but that some groups of neighboring assemblies had close to the same void fraction. To model the void fraction variation, the outer rows of assemblies were divided into six regions of approximately uniform water material density, and the average water density for the assemblies in each of these regions was calculated by multiplying the base water density (46.0415 lb/ft^3) by 1.0 minus the void fraction. The assemblies in each of these regions are indicated by the region numbers defined in Figure 3-1. The average region void fractions at midplane varied from about 2% to about 35% and are tabulated in Figure 3-1. Water density in the bypass region was taken to be the same as in the core except with zero void fraction. The downcomer water density was calculated for a temperature of 530 °F and a pressure of 1050 psia.

Neutron transport calculations were performed for two fuel cycles (cycles 7 and 12). The last cycle of irradiation for Capsule B was Cycle 12, and detailed information on this cycle was used to define the core model. The average power generated by each assembly was determined by the cycle burnup of each assembly supplied in Reference [3-4]. The power of the outer assemblies was then increased by the ratio of the power at axial midplane to the average assembly power determined from the calculated axial power profile at the midpoint of the cycle. The average of this ratio was 1.17. The individual pin powers were not used because NMPC chose to provide bundle average powers only. The power profile was assumed to be flat over each assembly. Neglect of the fall-off in pin power near the edge of the core will result in a slight increase in calculated flux.

The second fuel cycle that was used as input for the calculations was Cycle 7. This cycle was chosen because it had been previously calculated for the analysis of the 300 degree capsule [3-5]. Cycle 7 also is fairly typical of fuel cycles 1 through 11, whereas Cycle 12 has lower

power generation at the periphery of the core. Thus the Cycle 7 calculation can be used to estimate the effect on the flux magnitude of changing the fuel loading pattern, which affects the analysis of the dosimetry measurements. Examination of the three corner assemblies nearest the capsule indicates that the average relative power generation from these assemblies at midplane at mid-cycle is 0.42 for the first 11 cycles and is 0.39 for Cycle 7. However, for these particular assemblies, the Cycle 12 average is only slightly lower, 0.38. Thus, the effect of the lower peripheral power on the capsule flux level was not expected to be large.

For the Cycle 7 R-θ calculations, the same transport model was used as for Cycle 12, however, the relative assembly power generation and the void fraction data were changed as appropriate. A previous calculation by GE of the axial flux profile for Cycle 7 [3-6] used void fractions at midplane that are significantly higher than for Cycle 12. These higher void fractions were used for the Cycle 7 R-θ calculation.

The DOTSOR code (available as part of the LEPRICON code package [3-7]), was used to convert the cycle power distributions from x,y to R,θ coordinates and place the source in each mesh cell. The source per group was defined by an average fission spectrum calculated for a fission breakdown by isotope determined for the average burnup of the outer assemblies in Cycle 12. This is a good approximation to the fission spectrum because the outer assemblies were all burned assemblies and the fission spectrum only slowly varies with burnup. The average burnup was also used to determine the average value of the neutrons per fission and the average energy per fission.

A second transport calculation was performed for the Cycle 12 fuel pattern in R-Z geometry. For this calculation, the core was divided into 4 radial regions. Three of these regions consisted of each of the outer three rows of assemblies averaged over the octant. The fourth region consisted of the inner part of the core. Each radial region was divided into axial regions according to variation in void fraction. Both the power distribution and void fraction were given for each of the outer 4 rows of assemblies in 24 axial nodes [3-8]. Except for nodes near the bottom of the core which had zero void fraction, each node was modeled as a separate region. For convenience, cross sections were calculated for each region with void fractions rounded off to the nearest percent. This resulted in a total of 56 regions in the core with 42 distinct cross section sets. For the R-Z model, the core radius was taken to be that which gave the equivalent core volume. Regions above and below the core were not modeled exactly but consisted of a one-foot high water reflector with vacuum boundaries at the top and bottom of the model. The model had 142 mesh points in the radial direction as in the R-θ model except with slightly different boundaries near the core edge. In the axial direction, the model had 68 mesh points with 38 in the core region.

3.3 Neutron Transport Results

Selected flux results from the Nine Mile Point Unit 1 Cycles 7 and 12 neutron transport analyses are provided in Figures 3-2 and 3-3 and Tables 3-1 through 3-3. Figure 3-2 shows the

azimuthal variation of the flux above 1 MeV at the vessel inner radius (clad/base metal interface) at axial midplane for the two cycles. It is seen that at small angles, the Cycle 12 flux level is calculated to be about 19% lower than that of Cycle 7, while at larger angles there is less difference. This effect is due to the difference in power from the outer fuel assemblies that is pronounced in the assemblies nearer zero degrees. At the 30 degree capsule location, the difference is about 11%. Included in these differences is the effect of the difference in void fraction which contributes about 4% to 6% out of the 11% or 19% previously mentioned.

Tables 3-1 through 3-3 give the calculated fast neutron flux (E > 1 MeV) and (E > 0.1 MeV) and displacements per atom (dpa) per second for key points in the reactor vessel and at the center of the capsule at axial midplane. All values are normalized to the full power of 1850 MW thermal. These points include the vessel base metal surface, one quarter of the way through the vessel (1/4 T), half way through the vessel (1/2 T), and 3/4 of the way through the vessel (3/4 T). In the tables, IR stands for the inner radius of the vessel base metal (i.e., at the clad-base metal interface). The maximum flux at the vessel was found to occur near 17°. Values of flux at 0, 30, and 45 degrees are also included. The value at 30° is behind the capsule. The flux at this angle in octants without a capsule present will be higher since shielding by the capsule will be absent.

Table 3-4 gives the absolute calculated neutron flux spectrum at the center of the capsule for cycles 7 and 12. There is a bias in magnitude between the two, but little difference in spectrum shape. Except for the 4 highest energy groups, all the group fluxes are within about 1% of the values that would be determined by taking the ratio of flux above 1 MeV. The Cycle 12 spectrum was used for the Capsule B dosimetry analysis described in Section 3.4.

Comparisons were also made between the calculations reported here and the previous neutron spectrum calculations performed by Battelle for Cycle 7 which were made when the 300 degree capsule was first analyzed [3-5]. Because of changes in transport cross sections and the fission spectrum, some relative group fluxes differed by significant amounts between the two cases. However, in the most important energy range between 0.1 and 10 MeV, the differences were small. The spectral averaged dosimeter reaction cross sections for the iron, nickel, and copper reactions above 1 MeV were found to differ by about 4%. The newer calculation thus should produce measured fluence values that are 4% higher.

Figure 3-3 shows the result of the R-Z calculation. The axial flux profile is calculated to peak between 35 and 40 inches above midplane. The flux level at this point is indicated to be 45% higher than at midplane. This is considerably more than the value obtained by GE in the earlier Cycle 7 calculation of about 13% [3-6]. The cause of this difference is the differences between the axial power profiles for the two cycles.

Figure 3-4 shows the position of the beltline plates in the NMP-1 vessel for comparison to the axial flux profile. The axial position of the beltline plates, in relation to the core midplane, has been used to determine the peak fast neutron fluence in the lower shell course beltline plates.

Beltline plate G-8-1 is the surveillance plate. The determination of the flux to the lower shell course materials was calculated to confirm that plate G-8-1 is not the limiting material (i.e., plate G-8-1 does not have the highest ART). Further discussion concerning analysis of the beltline materials to determine the material with the limiting ART is provided later in this report.

3.4 Analysis of Dosimetry Data

3.4.1 Capsule B Dosimetry Analysis

The dosimetry from Capsule B consisted of three sets of Cu, Fe, and Ni wires. This dosimetry was counted to determine the fast neutron reactions as shown in Table 3-5. This table also gives the nuclear constants used to determine the reaction rates. These data are taken from the appropriate ASTM standards [3-9, 3-10, 3-11, 3-12]. The dosimetry results are tabulated in Table 3-6. The dosimeter measurements are presented in units of disintegrations per second (dps) adjusted to the end-of-irradiation (March 3, 1997 at 23:02). Using the power history, the ratio of reaction rate to dps was calculated, and the results are also in Table 3-6. The units of reaction rate are reactions per second per target nucleus. Since the dosimetry is all located at the center of the capsule in the radial and azimuthal directions, and close to the axial midplane of the reactor, no dosimeter gradient corrections are necessary.

Capsule B was irradiated from reactor start-up to March 1997 for a total of 16.76 effective full power years at 1850 MWt. The power history was supplied as the thermal generation per month over this period. The use of monthly power history data is not expected to introduce any significant error in the results, even for the relatively short-lived nickel reaction. However, there can be differences in fuel cycles which can introduce differences in flux to the capsule for the same power generation. In the earlier analysis of the Capsule B dosimetry [3-13], these differences were not included. In particular, the measured flux calculations were performed by assuming a constant ratio of flux to power. The only available transport data at the time the [3-13] work was performed was the previous Cycle 7 transport results, and these data were used to estimate the Cycle 12 measured fluxes.

In the current work, the measured fluxes were calculated by taking into account the change in flux to power ratio. In effect, the transport calculations for both Cycles 7 and 12 were used to interpret the dosimetry measurements to obtain a better interpretation of the measurements than that reported in [3-13]. To achieve this objective, it was assumed that the Cycle 7 calculated flux in the capsule is typical of cycles 1 to 11. As shown in Table 3-1, the Cycle 12 calculated flux is 11% lower than the calculated Cycle 12 flux. When the difference in cycle flux is accounted for, the ratio of copper reaction rate to wire count (dps/mg) increased by 7 %.

In summary, using the Cycle 12 calculated neutron spectrum at the center of the capsule (Table 3-4), together with reaction cross sections in 47 groups, along with the Cycle 7 flux, and power history, the flux above 1 MeV was determined for each dosimeter wire. The flux is given

by the measured reaction rate divided by the spectral averaged cross section above 1 MeV. The flux determined in this way for each dosimeter, and the average for each of the three dosimeter types, is given in Table 3-6. The results indicate that a consistent difference is observed between the three monitors, while the individual monitors of the same type are in good agreement. The dosimeter material differences are indicative of differences in flux level in the capsule at full power, both within Cycle 12 and between cycles, and these differences result from effects that have not been included in the calculations. The most important of these effects are differences in magnitude of the void fraction in the outer assemblies and changes in the axial power profile and void fraction during the cycle.

3.4.2 Comparison of 210 and 300 Degree Capsules

Comparison of the Capsule B dosimetry results may be made with earlier results from the capsule at 300 degrees presented in Reference [3-5]. In the earlier case, good agreement was observed among the different dosimeter reactions. Thus, the Capsule B dosimeter result differences are not typical of earlier capsules. Since the dosimeter data and transport calculations indicate that the fast flux at the midplane has decreased since the end of Cycle 7, it is recommended that only the copper reaction be used for Capsule B exposure determination, since only this reaction is sensitive to fluence from any but the last cycle or two. Therefore, the recommended average flux for Capsule B (average copper value from Table 3-6) is 1.895E09 n/cm^2/s (averaged over all 12 cycles). The recommended value from the 300 degree capsule was 1.90E09 n/cm^2/s, which is in good agreement. Because the data indicate the Cycle 12 flux to be lower than that for Cycle 7, the average flux for Capsule B should be slightly lower than the earlier value. Recommended values for exposure for Capsule B based on the average of the copper measurements are given in Table 3-7.

The dosimetry difference between the nickel and iron reactions cannot be resolved by cycle differences in relative exposure. However, there may be effects within Cycle 12 that can explain the observations. In contrast to Cycle 7, the cycle 12 axial flux profile is peaked above midplane in the outer assemblies, which is probably due to previous burnup to higher levels in the bottom half of the assemblies. Further power shifts upward might lower the midplane power value and drop the capsule flux as the cycle progresses. This is exactly what the relatively short half-life nickel monitor indicates.

Even with the cycle power adjustment using the Cycle 7 to Cycle 12 calculated flux difference, the iron and copper monitors do not agree, although the correction did eliminate a substantial part of the discrepancy. The iron monitor mainly responds to the last cycle and the copper monitor to the last 4 cycles. The lower nickel result indicates that the iron monitor response should also be biased low due to greater radioactive decay for activation at the beginning of the cycle. Also, the representation of cycles 8-11 using the cycle 7 power distribution and void fraction data may not be accurately representing the capsule flux differences.

Although the power history effects are the most likely cause of the differing monitor response, uncertainty in the calculated neutron spectrum is also a possible contributor. The calculations do not predict any significant change in spectrum. Although spectrum uncertainties can affect the evaluation of the relative response of the iron and copper monitors, the iron and nickel response is so similar that no realistic spectrum error can resolve the differences observed. Thus the analysis here has assumed that the three dosimeter reactions do not provide any data to indicate that the calculated neutron spectrum shape should be adjusted.

Comparisons of the "measured" flux values for the 210 and 300 degree capsules, with the absolute calculations reported in the preceding section, indicates that the 300 degree capsule flux measurement is higher than the Cycle 7 calculation by 9%, and the 210 degree capsule measurement is higher than the Cycle 12 calculation by 21%. If the iron Capsule B dosimetry result (which is mostly sensitive to the Cycle 12 flux level) is factored into the comparison with the Cycle 12 calculation, the agreement would be closer. In fact, by correcting for the earlier cycle contributions at higher flux levels, the bias is found to be about 10%, showing the consistency between the two capsules as already discussed above. For conservatism, the 9-10% bias was used for fluence evaluation in the vessel (see Section 3.5).

3.4.3 Capsule Fluence Uncertainty Analysis

An uncertainty estimate was made for the Capsule B fluence determination. The main sources of uncertainty are the calculated neutron flux spectrum in the capsule, and the deviation in flux history after cycle 7. Use of the copper monitor alone provides only a normalization of the calculated fluence and no check on the accuracy of the calculated neutron spectrum. Based on experience with other capsules (Reference [3-14]), the flux ($E > 1$ MeV) uncertainty due to the neutron spectrum uncertainty is conservatively estimated to be 12%. An estimate of the power history uncertainty effect was derived from the changes necessary to allow the copper and iron reactions to be in agreement. This change affected the copper reaction rate by 7%. The 7% value was chosen to be an estimate of the 1σ uncertainty from this source. Combining the two uncertainties in quadrature results in an overall uncertainty of 14%.

Other uncertainties are present but are not significant contributors to the overall uncertainty. The downcomer water temperature has an uncertainty of $\pm$ 5°F which results in about a 2.8% uncertainty in calculated capsule flux. Bigger uncertainties in calculated flux arise from uncertainty in the void fraction in the outer assemblies. However, these factors do not have any appreciable effect on the neutron spectrum, and so do not affect the flux derived from the dosimetry. Uncertainties in water densities and variation in these densities with time can affect the relative flux at the capsule and the ratio of flux at the vessel to the capsule. These uncertainties are included in the vessel analysis in the following section of this report.

3.5 Vessel Fluence Evaluation and Projection

3.5.1 R-Z Transport Results

In order to calculate P-T curves, it is necessary to determine the vessel exposure at the maximum point. From the R-θ calculation results, the maximum point occurs at an azimuthal angle of 17 degrees. The maximum point in the axial direction is determined by the axial power profile and the axial variation of the void fraction in the outer assemblies. A previous calculation of the axial flux shape for Cycle 7 [3-6] indicated that the location of the maximum was at 100 inches from the bottom of the core and the position of this maximum did not change significantly during the cycle. The ratio of vessel flux at the maximum position to that at the axial midplane was calculated by GE to be 1.138. This value was taken to be typical of cycles 1-11. For Cycle 12, an R-Z calculation was performed using a significantly different power shape. This resulted in a value of the axial peak flux which is 44.6% higher than the value of flux at midplane at a location 107 to 112 inches above the bottom of the core.

The vessel fluence and dpa were evaluated for the end of Cycle 12 (16.76 EFPY) and for 28 EFPY. These exposure data are given in Table 3-8. To derive the values at the maximum point on the vessel inner radius, the exposure through the end of Cycle 11 was calculated by increasing the Cycle 7 calculated flux magnitude by the axial peaking factor relative to midplane (1.138) and by a bias factor of 1.09. As discussed earlier, the bias factor was determined by comparing the 300 degree and 210 degree capsule measured and calculated data. For Cycle 12 and projections into the future, the Cycle 12 flux magnitude was used with the axial peaking factor of 1.446 and a capsule bias factor of 1.10. While these factors increase the flux at the maximum point relative to previous cycles, the lower calculated capsule flux for Cycle 12, and the lower azimuthal peak relative to the capsule, largely offset the increase. The end result of the lower calculated midplane vessel fluence at 17 degrees relative to the capsule, and the higher axial peaking factor, was an increase of the flux at the peak vessel point of 3% relative to the Cycle 7 value. The extrapolation for future exposure assumes that future fuel cycles will be similar to Cycle 12, which is conservative since the Cycle 12 flux is higher. The conservative assumption is also made that the peak vessel flux is at the same point in all cycles.

3.5.2 In-vessel Peak Fluence Calculations

To evaluate the effect of exposure within the vessel, RG1.99(2) requires the use of the more conservative dpa attenuation applied to fluence (E > 1 MeV). Values of fluence above 1 MeV using this attenuation are given in Table 3-9. These values are derived using two methods: (1) from the plant-specific calculated dpa attenuation given in Table 3-8; and (2), using the RG1.99(2) attenuation factor (attenuation of exp(-.24x), with x the depth into the vessel in inches). If the generic RG1.99(2) formula is used in place of the plant-specific dpa results, the fluence would be ~3% lower at the 1/4 T position, but ~20% higher at the 3/4 T depth. Since RG1.99(2) allows either the use of the dpa attenuation formula or plant-specific data, and since the effect of the difference on the leak/hydrotest curve is negligible when either is used, the

generic RG1.99(2) dpa attenuation has been used in the P-T curves.

As discussed in Chapter 4, determination of the limiting beltline plate was performed using a lower fluence for beltline plates located below the core midplane. These fluences were calculated using the R-Z transport results referenced to the peak position above the core midplane. These data are given in Table 3-10. As shown in the table for Cycle 12, lower shell course plates which are located 42.19 inches below the core midplane, experience a fluence which is 0.4 times the peak fluence of the upper shell course. In Cycle 7, the lower shell course plates experienced a flux which is 0.67 times the peak fluence of the upper shell course plates [3-6]. In order to ensure conservative, but accurate results, the 0.67 factor was applied to cycles 1 through 11 and the 0.4 factor was applied to cycles 12 through 28. Thus, the maximum fluence in the lower shell course for 28 EFPY is 0.545 times the peak fluence in the upper shell course based on the time weighted flux values.

3.5.3 Vessel Fluence Uncertainty Analysis

Uncertainties in the vessel fluence are larger than for the capsule fluence because of the additional extrapolation from the dosimetry measurement points. Because of the closeness of the capsule to the vessel, this extrapolation is small near the capsule angle, but larger error can be present in the extrapolation axially and azimuthally to the maximum flux point. This error was investigated by varying the void fraction in the calculations, and by looking at the axial and azimuthal flux shape differences between Cycle 7 and Cycle 12. Estimated uncertainty in the peaking factors was also included. Combining these uncertainties results in an estimated extrapolation uncertainty of 11%. The total uncertainty in the peak vessel flux determination is found by combining in quadrature the capsule fluence uncertainty of 14% and the extrapolation uncertainty. This results in a total uncertainty of 18% for the peak vessel fluence.

3.6 Chapter 3 References

[3-1] RSICC Computer Code Collection, CCC-543, TORT-DORT-PC, Two- and Three-Dimensional Discrete Ordinates Transport Version 2.7.3, available from the Radiation Safety Information Computational Center, Oak Ridge National Laboratory, Oak Ridge, TN, June 1996.

[3-2] RSICC Data Library Collection, DLC-185, BUGLE-96, Coupled 47 Neutron, 20 Gamma Ray Group Cross Section Library Derived from ENDF/B-VI for LWR Shielding and Pressure Vessel Dosimetry Applications, available from the Radiation Safety Information Computational Center, Oak Ridge National Laboratory, Oak Ridge, TN, March 1996.

[3-3] ASTM Designation E482-89, *Standard Guide for Application of Neutron Transport Methods for Reactor Vessel Surveillance*, in ASTM Standards, Section 12, American Society for Testing and Materials, Philadelphia, PA, 1997.

[3-4] Letter SA-98-8, Anthony M. Salvagno to M.P. Manahan, "Data for NMP-1 Neutron Transport Analysis", Feb. 10, 1998.

[3-5] D. Stahl, et. al., "Final Report on Examination, Testing and Evaluation of Irradiated Pressure Vessel Surveillance Specimens from the Nine Mile Point Nuclear Power Station", BCL-585-84-6, Battelle Memorial Institute, 505 King Avenue, Columbus, Ohio 43201, July 1984.

[3-6] L.S. Burns and D.R. Rogers, "Fast Neutron Axial Pressure Vessel Calculations for Nine Mile Point Unit No. 1", MDE Report 236-1085, Rev. 1, Jan. 21, 1986.

[3-7] RSICC Peripheral Shielding Routine Code Collection, PSR-277, LEPRICON, PWR Pressure Vessel Surveillance Dosimetry Analysis System, available from the Radiation Safety Information Computational Center, Oak Ridge National Laboratory, Oak Ridge, TN, June 1995.

[3-8] Letter FA98-32, Anthony M. Salvagno to M.P. Manahan, "Data for NMP-1 Neutron Transport Analysis-Final", April 8, 1998.

[3-9] ASTM Designation E263-88, *Standard Method for Determining Fast-Neutron Flux Density by Radioactivation of Iron*, in ASTM Standards, Section 12, American Society for Testing and Materials, Philadelphia, PA, 1997.

[3-10] ASTM Designation E264-92, *Standard Method for Determining Fast-Neutron Flux Density by Radioactivation of Nickel*, in ASTM Standards, Section 12, American Society for Testing and Materials, Philadelphia, PA, 1997.

[3-11] ASTM Designation E523-87, *Standard Method for Determining Fast-Neutron Flux Density by Radioactivation of Copper*, in ASTM Standards, Section 12, American Society for Testing and Materials, Philadelphia, PA, 1997.

[3-12] ASTM Designation E1005-84, *Standard Test Method for Application and Analysis of Radiometric Monitors for Reactor Vessel Surveillance,* in ASTM Standards, Section 12, American Society for Testing and Materials, Philadelphia, PA, 1997.

[3-13] Report MPM-398675 to Niagara Mohawk, "Nine Mile Point Unit 1 210° Surveillance Capsule Report", March 1998.

[3-14] E. P. Lippincott, "Westinghouse Surveillance Capsule Neutron Fluence Reevaluation", WCAP-14044, Westinghouse Electric Corporation, PO Box 355, Pittsburgh, Pa 15230, April 1994.

Table 3-1 Calculated Core Midplane Flux (E > 1.0 MeV) (n/cm²-s) at Selected Locations

Cycle 12 Calculation				
Location	0°	17°	30°	45°
Vessel IR	1.46e+09	1.92e+09	1.32e+09	8.60e+08
Vessel 1/4 T	9.37e+08	1.23e+09	8.16e+08	5.54e+08
Vessel ½ T	5.25e+08	6.82e+08	4.57e+08	3.11e+08
Vessel 3/4 T	2.73e+08	3.53e+08	2.38e+08	1.62e+08
Capsule			1.56e+09	
Cycle 7 Calculation				
Location	0°	17°	30°	45°
Vessel IR	1.80e+09	2.39e+09	1.48e+09	8.68e+08
Vessel 1/4 T	1.15e+09	1.52e+09	9.15e+08	5.59e+08
Vessel 1/2 T	6.47e+08	8.47e+08	5.12e+08	3.14e+08
Vessel 3/4 T	3.36e+08	4.37e+08	2.67e+08	1.64e+08
Capsule			1.75e+09	

Table 3-2 Calculated Core Midplane Flux (E > 0.1 MeV) (n/cm²-s) at Selected Locations

Cycle 12 Calculation				
Location	0°	17°	30°	45°
Vessel IR	2.78e+09	3.66e+09	2.70e+09	1.63e+09
Vessel 1/4 T	2.43e+09	3.17e+09	2.26e+09	1.43e+09
Vessel 1/2 T	1.79e+09	2.31e+09	1.65e+09	1.05e+09
Vessel 3/4 T	1.15e+09	1.47e+09	1.05e+09	6.76e+08
Capsule			2.83e+09	
Cycle 7 Calculation				
Location	0°	17°	30°	45°
Vessel IR	3.43e+09	4.56e+09	3.03e+09	1.64e+09
Vessel 1/4 T	3.00e+09	3.94e+09	2.54e+09	1.44e+09
Vessel 1/2 T	2.21e+09	2.87e+09	1.86e+09	1.07e+09
Vessel 3/4 T	1.42e+09	1.82e+09	1.19e+09	6.84e+08
Capsule			3.17e+09	

Table 3-3 Calculated Core Midplane dpa/s at Selected Locations

Cycle 12 Calculation				
Location	0°	17°	30°	45°
Vessel IR	2.26e-12	2.95e-12	2.05e-12	1.34e-12
Vessel 1/4 T	1.53e-12	1.98e-12	1.35e-12	9.07e-13
Vessel 1/2 T	9.41e-13	1.21e-12	8.38e-13	5.59e-13
Vessel 3/4 T	5.36e-13	6.87e-13	4.80e-13	3.19e-13
Capsule			2.38e-12	
Cycle 7 Calculation				
Location	0°	17°	30°	45°
Vessel IR	2.78e-12	3.66e-12	2.29e-12	1.36e-12
Vessel 1/4 T	1.88e-12	2.46e-12	1.52e-12	9.16e-13
Vessel 1/2 T	1.16e-12	1.51e-12	9.40e-13	5.65e-13
Vessel 3/4 T	6.61e-13	8.52e-13	5.39e-13	3.23e-13
Capsule			2.67e-12	

Table 3-4 Calculated Neutron Flux Spectrum at the Center of Capsule B

Calculated 47 Group Neutron Spectrum at Capsule Center							
Group	Energy	Cycle 12 n/cm²/s	Cycle 7 n/cm²/s	Group	Energy	Cycle 12 n/cm²/s	Cycle 7 n/cm²/s
1	1.733E+01	1.702e+06	1.858e+06	25	2.972E-01	2.026e+08	2.286e+08
2	1.419E+01	4.694e+06	5.148e+06	26	1.832E-01	1.790e+08	2.020e+08
3	1.221E+01	1.608e+07	1.772e+07	27	1.111E-01	1.373e+08	1.548e+08
4	1.000E+01	2.837e+07	3.136e+07	28	6.738E-02	1.074e+08	1.213e+08
5	8.607E+00	4.312e+07	4.784e+07	29	4.087E-02	4.242e+07	4.805e+07
6	7.408E+00	1.075e+08	1.196e+08	30	3.183E-02	2.812e+07	3.180e+07
7	6.065E+00	1.349e+08	1.505e+08	31	2.606E-02	3.194e+07	3.604e+07
8	4.966E+00	1.961e+08	2.194e+08	32	2.418E-02	2.004e+07	2.259e+07
9	3.679E+00	1.203e+08	1.347e+08	33	2.188E-02	6.498e+07	7.329e+07
10	3.012E+00	7.932e+07	8.894e+07	34	1.503E-02	1.107e+08	1.248e+08
11	2.725E+00	8.437e+07	9.468e+07	35	7.102E-03	1.305e+08	1.472e+08
12	2.466E+00	3.990e+07	4.481e+07	36	3.355E-03	1.151e+08	1.298e+08
13	2.365E+00	9.728e+06	1.094e+07	37	1.585E-03	1.809e+08	2.040e+08
14	2.346E+00	4.854e+07	5.454e+07	38	4.540E-04	1.073e+08	1.209e+08
15	2.231E+00	1.234e+08	1.385e+08	39	2.145E-04	1.068e+08	1.204e+08
16	1.920E+00	1.238e+08	1.389e+08	40	1.013E-04	1.401e+08	1.579e+08
17	1.653E+00	1.632e+08	1.832e+08	41	3.727E-05	1.699e+08	1.917e+08
18	1.353E+00	2.345e+08	2.633e+08	42	1.068E-05	9.910e+07	1.118e+08
19	1.003E+00	1.442e+08	1.620e+08	43	5.044E-06	1.294e+08	1.457e+08
20	8.208E-01	7.579e+07	8.507e+07	44	1.855E-06	9.508e+07	1.069e+08
21	7.427E-01	1.862e+08	2.093e+08	45	8.764E-07	8.140e+07	9.114e+07
22	6.081E-01	1.405e+08	1.580e+08	46	4.140E-07	1.248e+08	1.388e+08
23	4.979E-01	1.660e+08	1.870e+08	47	1.000E-07	1.107e+09	1.222e+09
24	3.688E-01	1.431e+08	1.609e+08				

Table 3-5 Nuclear Parameters Used in the Evaluation of Neutron Sensors

Monitor Material	Reaction of Interest	Target Fraction	Approx. Response Threshold	Product Half-Life
Copper	$Cu^{63}(n,\alpha)Co^{60}$	0.6917	5 MeV	5.271 yrs
Iron	$Fe^{54}(n,p)Mn^{54}$	0.0580	2 MeV	312.5 days
Nickel	$Ni^{58}(n,p)Co^{58}$	0.6827	2 MeV	70.78 days

Table 3-6 Tabulation of Capsule B Dosimetry Results

Wire	dps/mg	Reaction Rate	Flux (E > 1) ($n/cm^2/s$)
Cu-1	20.66	4.947e-18	1.928e+09
Cu-2	20.81	4.983e-18	1.942e+09
Cu-3	19.43	4.653e-18	1.813e+09
Avg	20.30	4.861e-18	1.895e+09
Fe-1	149.4	2.958e-16	1.734e+09
Fe-2	138.6	2.745e-16	1.609e+09
Fe-3	135.7	2.687e-16	1.575e+09
Avg	141.2	2.797e-16	1.639e+09
Ni-1	1725	2.979e-16	1.363e+09
Ni-2	1636	2.825e-16	1.293e+09
Ni-3	1592	2.749e-16	1.258e+09
Avg	1651	2.851e-16	1.305e+09

Table 3-7 Recommended Exposure Values for Capsule B

Flux (E> 1.0 MeV)	1.895e+09	$n/cm^2/s$
Flux (E> 0.1 MeV)	3.43e+09	$n/cm^2/s$
dpa/s	2.89e-12	/s
Fluence (E > 1.0 MeV)	1.00e+18	n/cm^2
Fluence (E > 0.1 MeV)	1.81e+18	n/cm^2
dpa	0.00153	

Table 3-8 Estimated Maximum Exposure in the Reactor Vessel Wall of the Nine Mile Point Unit 1 Reactor

	Fluence (E>1 MeV) n/cm^2	Fluence (E>0.1 MeV) n/cm^2	dpa
Maximum Vessel Exposure at end of Cycle 12 (March 1997)			
IR	1.57e+18	2.99e+18	2.41e-03
1/4 T	1.00e+18	2.59e+18	1.62e-03
1/2 T	5.56e+17	1.89e+18	9.88e-04
3/4 T	2.87e+17	1.20e+18	5.59e-04
Maximum Vessel Exposure at 28 EFPY			
IR	2.64e+18	5.05e+18	4.06e-03
1/4 T	1.69e+18	4.37e+18	2.73e-03
1/2 T	9.39e+17	3.19e+18	1.67e-03
3/4 T	4.85e+17	2.02e+18	9.45e-04

Note: The data in this table are based on the assumption that the cycle 7 flux applies through the end of cycle 11 and the cycle 12 flux applies after cycle 11. As discussed in Section 4, the P-T curve calculations were performed using the cycle 12 flux from reactor startup which is conservative.

Table 3-9 Maximum Vessel Fluence (E > 1 MeV) Using dpa Attenuation

Position	16.76 EFPY Fluence (n/cm^2)		28 EFPY Fluence (n/cm^2)	
	Calculated dpa	RG1.99(2)	Calculated dpa	RG1.99(2)
IR	1.57e+18	1.57e+18	2.64e+18	2.64e+18
1/4 T	1.05e+18	1.02e+18	1.78e+18	1.72e+18
½ T	6.43e+17	6.66e+17	1.09e+18	1.12e+18
3/4 T	3.64e+17	4.34e+17	6.15e+17	7.33e+17

Note: The data in this table are based on the assumption that the cycle 7 flux applies through the end of cycle 11 and the cycle 12 flux applies after cycle 11. As discussed in Section 4, the P-T curve calculations were performed using the cycle 12 flux from reactor startup which is conservative.

Table 3-10 Cycle 12 Relative Axial Flux (E > 1.0 MeV) Variation in the Core Region

Distance from Midplane (in)	Relative Flux (E > 1.0 MeV)	Distance from Midplane (in)	Relative Flux (E > 1.0 MeV)
-71.85	0.132	3.00	0.721
-71.45	0.136	9.00	0.783
-70.85	0.143	15.00	0.847
-70.12	0.152	21.00	0.909
-69.38	0.161	27.00	0.961
-68.25	0.174	33.00	0.995
-66.75	0.192	39.00	1.000
-64.50	0.218	45.00	0.965
-61.50	0.253	51.00	0.883
-57.00	0.299	57.00	0.758
-51.00	0.347	61.50	0.636
-45.00	0.385	64.50	0.545
-39.00	0.420	66.75	0.480
-33.00	0.453	68.25	0.434
-27.00	0.487	69.38	0.403
-21.00	0.524	70.12	0.381
-15.00	0.565	70.85	0.360
-9.00	0.611	71.45	0.343
-3.00	0.663	71.85	0.332

Note: The axial flux profile has been calculated relative to the peak flux position.

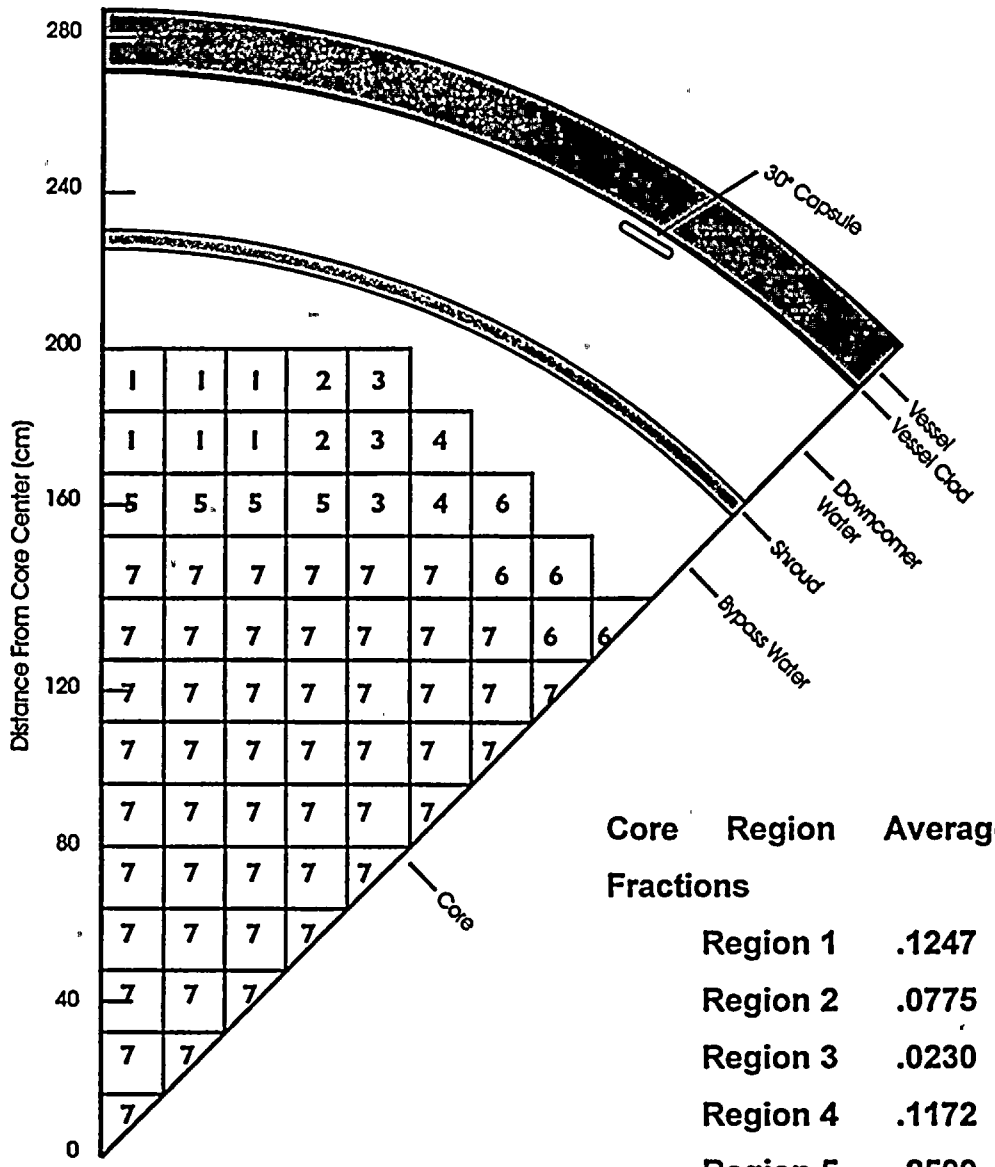

Core Region Average Void Fractions	
Region 1	.1247
Region 2	.0775
Region 3	.0230
Region 4	.1172
Region 5	.2599
Region 6	.1922
Region 7	.3543

Figure 3-1 Nine Mile Point Unit 1 R-θ Geometry Used in the DORT Calculations

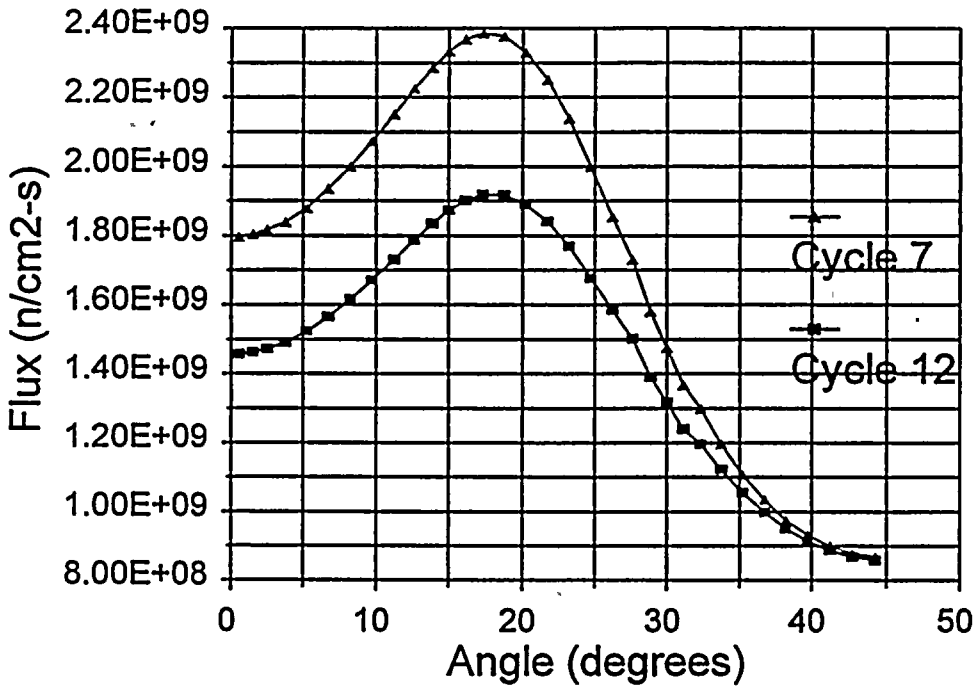

Figure 3-2 **Calculated Azimuthal Flux (E > 1.0 MeV) Variation at the Reactor Vessel Inner Radius for Cycle 7 and Cycle 12**

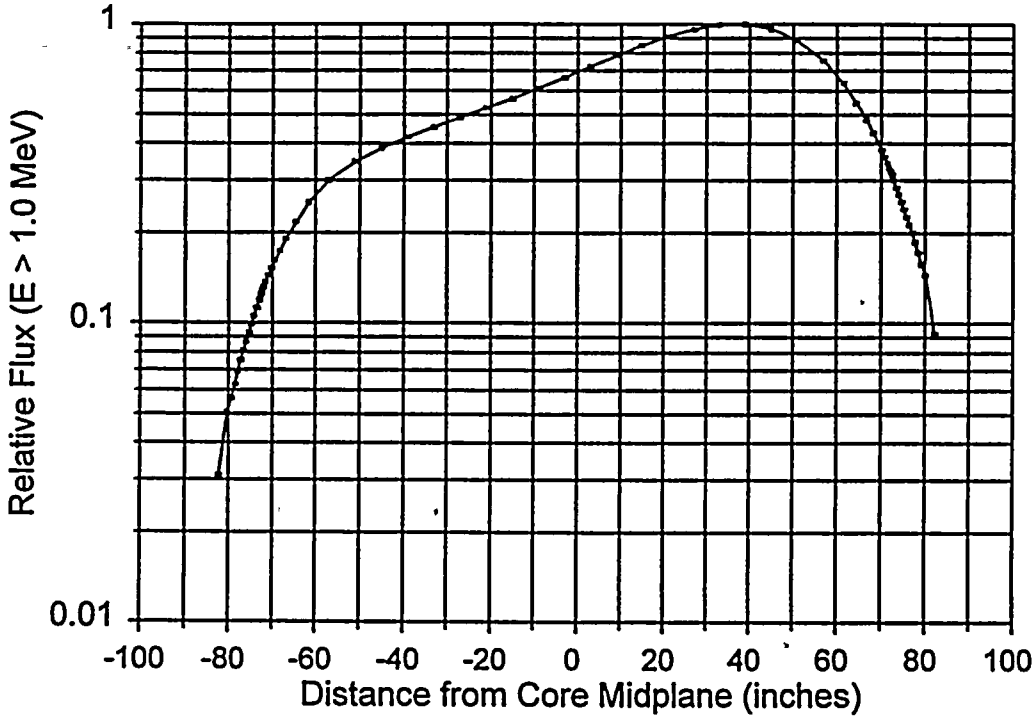

Figure 3-3 · Calculated Axial Flux (E > 1.0 MeV) Variation at the Reactor Vessel Inner Radius for Cycle 12

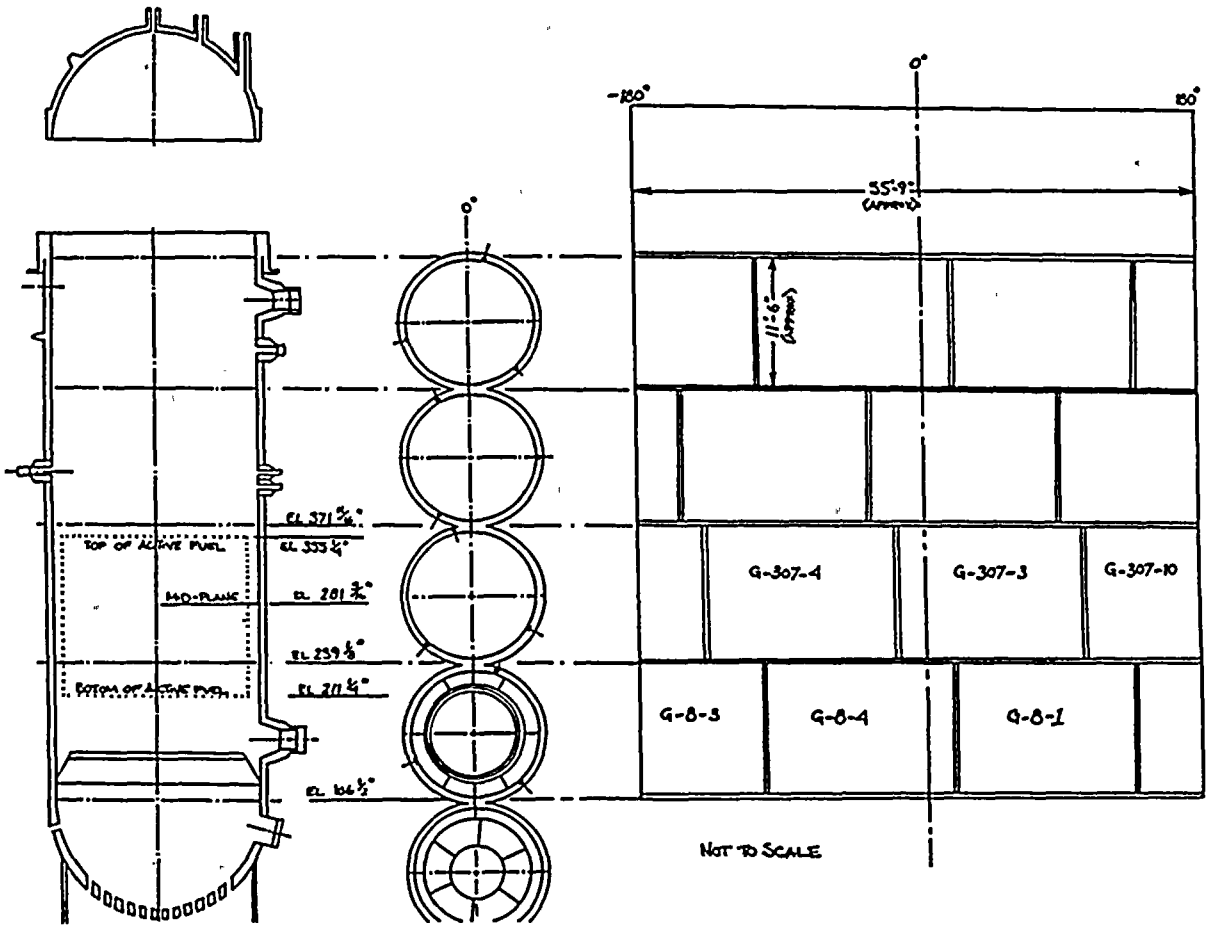

Figure 3-4 **Drawing Showing the Axial Position of the NMP-1 Beltline Plates Relative to the Core Midplane**

4.0 Pressure-Temperature Curve Analysis

P-T curves for up to 28 effective full power years (EFPY) were calculated for NMP-1. In addition, leak/hydro test curves were calculated at 20 EFPY and at 24 EFPY. These additional leak/hydro test curves were calculated in an effort to minimize outage time since heatup to the leak/hydro test temperature is slow in a BWR.

This section of the report contains a brief review of the data development necessary to calculate the P-T curves as well as the P-T curves themselves.

4.1 Neutron Fluence Determination

Two dimensional discrete ordinates transport calculations for NMP-1 were reported in Section 3.0. The cycle 12 peak ID fast (E > 1 MeV) flux was determined to be 3.054×10^9 n/cm^2/sec. This flux, which is 3% higher than the peak cycle 7 flux, was assumed to represent the exposure from plant startup through 28 EFPY for the upper shell course plates. Therefore, at 28 EFPY, the peak ID surface fast fluence will be 2.70×10^{18} n/cm^2.

Using the Reference [4-1] attenuation factor with a vessel wall thickness x = 7 1/8 in (base metal), the 1/4 T fluence is:

$$\phi t_{1/4\ T} = [2.70 \times 10^{18}\ n/cm^2]\ \exp\left[-0.24\left(\frac{7.125}{4}\right)\right]$$
$$= 1.759 \times 10^{18}\ n/cm^2$$

and the 3/4 T fluence is:

$$\phi t_{3/4\ T} = [2.70 \times 10^{18}\ n/cm^2]\ \exp\left[-0.24\ (7.125)\left(\frac{3}{4}\right)\right]$$
$$= 7.479 \times 10^{17}\ n/cm^2$$

4.2 Surveillance Data Assessment

The method of RG1.99(2) was used to evaluate the surveillance plate data. Three data points are available for plate G-8-1, and the results are presented in Table 4-1 [3-13]. In the application of these data to the NMP-1 vessel, the weight given to them depends on the credibility of the surveillance data as judged by the five criteria given in the regulatory guide. Based on the copper and nickel content of the vessel beltline plates, the surveillance plate is not the limiting material since plate G-307-4 has higher copper and nickel content and a higher initial RT_{NDT}. Therefore, the surveillance plate materials do not meet the first criterion that the

materials in the capsule should be judged to be controlling with regard to radiation embrittlement. Despite this fact, Position 2.1 of the regulatory guide was used to calculate the plate ART value.

The three surveillance plates were fitted according to the RG 1.99(2) procedure to the following equation:

$$CF = \frac{(Shift_{30}*FF_{30}+Shift_{210}*FF_{210}+Shift_{300}*FF_{300})}{(FF_{30}^2+FF_{210}^2+FF_{300}^2)}$$

where,

$Shift_i$ = Charpy 30 ft-lb shift for capsule i
FF_i = RG 1.99(2) fluence factor for capsule i

The resulting least-squares fit for the surveillance CF (221.26 F) is larger than the Table CF (153.95) for this material. Criterion 3 evaluates the scatter about the mean CF value and scatter from the mean for the base metal should be within 17 F for credible data. As shown in Table 4-1, one data point (300 degree capsule point) exceeds the predicted value by 21.19 F. Therefore, Criterion 3 is not satisfied for the G-8-1 surveillance plate material and the full 34 F margin term must be used. The CF + 34 F prediction bounds all the surveillance data points.

The applicability of the RG1.99(2) Table CF for analysis of the beltline materials was assessed by comparing the measured plate G-8-1 data to the RG1.99(2) model plus 34 F bound. The results are shown in Table 4-2. Only one surveillance data point falls outside of the RG 1.99(2) model (Table CF) plus 2 sigma margin for plate G-8-1, and this point exceeds the 2 sigma limit by only 6.5 F. The other two surveillance points are comfortably bounded by the RG1.99(2) model. Based on this comparison, it was concluded that application of the RG1.99(2) model using the Table CF + 34 F margin is appropriate for the other beltline plates.

4.3 ART For Limiting RPV Material

P-T curve calculations are performed using mechanical property data for the RPV material which is limiting over the operating period for which the P-T curves are valid. Using the RG1.99(2) procedure, the beltline plate with the largest ART is limiting for the beltline region. The initial RT_{NDT} data for the beltline materials is summarized in Table 4-3.

The procedure for ART calculation described in RG1.99(2) was used to determine the ART of the beltline materials. The ART at 28 EFPY is given by:

$$ART = RT_{NDT} + \Delta RT_{NDT} + Margin$$

The mean ΔRT_{NDT} is calculated using:

$$\Delta RT_{NDT} = CF \times FF \ (°F)$$

where,

CF	=	RG1.99(2) chemistry factor (F), either from the Tables or from the surveillance data fitting procedure
FF	=	RG1.99(2) fluence factor = $f^{(0.28 - 0.1 \log f)}$
f	=	fast neutron fluence in units of 10^{19} n/cm^2
Margin	=	$2(\sigma_\Delta^2 + \sigma_I^2)^{0.5}$
σ_Δ	=	28 F for welds and 17 F for plates
σ_I	=	standard deviation for initial RT_{NDT}

The results of the ART calculation are given in Table 4-4. Since plates G-8-1 and G-8-3/4 lie 42 inches below the core midplane, and the cycle average peak flux occurs ~ 27 inches or more above core midplane, the upper bound flux for plates G-8-1 and G-8-3/4 determined from the Cycle 7 and Cycle 12 neutron transport analysis was used in the ART calculation. Table 4-4 show that the limiting material is plate G-307-4/5.

With regard to the non-beltline materials, the NMP-1 FSAR states that the RT_{NDT} (L-T orientation) does not exceed 40°F for any of the non-beltline steels. Therefore, conservatively assuming a 30°F LT to TL additive conversion, the RT_{NDT} of the non-beltline material is below 70°F which is significantly below any beltline material. Therefore, plate G-307-4 is the limiting vessel material.

4.4 Thermal Transient Analysis

The temperature gradients in the pressure vessel wall at several heating and cooling rates were determined by transient thermal analyses using the TRUMP [4-3] computer program which has been integrated into the PT Curve Version 1.0 computer program [4-4]. The pressure vessel wall was modeled as a cylinder having an internal radius of 106.34 inches and a wall thickness of 7.28 inches to conservatively include the effects of the clad. The pressure vessel wall was divided into 17 nodal elements. The inner nodal element was thermally coupled with a high thermal coefficient to a boundary node whose temperature change was controlled at the desired heating or cooling rates. The outer surface of the outer nodal element and the ends of all nodal elements were modeled as adiabatic surfaces, i.e., no heat flow through these surfaces. Six heating and cooling rates were evaluated. These included 0, 20, 40, 60, 80, and 100°F per hour. For each of the heating studies, the model was set at a uniform temperature of 70°F and heated up to 550°F. For each of the cooling studies, the model was initially set at a uniform temperature of 550°F and cooled at a constant rate to 70°F. The temperature difference through the RPV wall and the temperature difference between the ID surface and the 1/4 T and 3/4 T positions were calculated every 1°F of the thermal transient ramp for each heatup and cooldown rate. These data were provided as input to the P-T curve calculations.

4.5 Minimum Temperature for Critical Core Operation

Appendix G to 10CFR50 requires that when the core is critical the RPV temperature must exceed the minimum permissible temperature (T_{CRIT}) for in-service system hydrostatic pressure test. Using the ASME reference stress intensity factor relation, the minimum metal temperatures for core critical operation are:

$$T_{CRIT}\Big|_{1/4\ T} = 248°F$$

$$T_{CRIT}\Big|_{3/4\ T} = 217°F$$

During cooldown, the 1/4 T position is limiting because the membrane and tensile stresses are additive and higher than those at the 3/4 T. The coolant temperature (T_c) which corresponds to T_{CRIT} can be calculated as follows:

$$T_c\ (\text{cooldown}) = T_{CRIT}\Big|_{1/4\ T} - \Delta T_{1/4\,T} + T_{error}$$

$$T_c\ (\text{cooldown}) = 260\ °F$$

During heatup, the 3/4 T limits at 100°F/hr. We have:

$$T_c\ (\text{heatup}) = T_{CRIT}\Big|_{3/4\ T} + \Delta T_{3/4\,T} + T_{error}$$

$$T_c\ (\text{heatup}) = 278\ °F$$

The limit for core operation is then determined by drawing a vertical line on the pressure temperature curve, intersecting a curve 40°F higher than the non-critical P-T limit curve for heatup and cooldown operations in accordance with 10CFR50, Appendix G.

4.6 Summary of Plant Parameters

There are several key plant parameters which are used in P-T curve calculations. These parameters are summarized in Table 4-5. The instrumentation used to measure reactor vessel pressure during plant heatup, cooldown, and leak/hydro testing are documented in [4-5].
For heatup/cooldown, the pressure measurement uncertainty used in the P-T calculations is ±52.2 psig and the temperature measurement uncertainty is ±12.2°F. For leak/hydro test, the pressure measurement uncertainty used in the P-T calculations is ±10.0 psig and the temperature measurement uncertainty is ±4.0°F. These uncertainties have been included in the P-T curves and Tables.

4.7 P-T Curves

The P-T curve equations have been incorporated into the MPM Technologies, Inc. computer code called PT Curve [4-4]. The results of the analyses are provided in Figures 4-1 through 4-7 and in Tables 4-6 through 4-12.

The leak/hydro test curve was calculated in accordance with 10CFR50, Appendix G which specifies that there should be no thermal gradient load applied during hydrotest. Therefore, during leak/hydro test, the non-critical heatup curve should be used to achieve the desired temperature, and then, after the appropriate soak time, the leak/hydro test curve may be used to pressurize the vessel to the desired test pressure. After the test is completed, the heatup/cooldown curves must be used since a temperature change is anticipated.

As described in Section 2.0, heating rates up to 100°F per hour have been analyzed to obtain the most limiting conditions. Lower bound curves from heating/cooling rates up to 100°F/hr, in conjunction with the specifications of 10CFR50 Appendix G, were used to obtain the P-T curve shown in Figures 4-1 through 4-5. In accordance with the guidance provided in 10CFR50 Appendix G, a total of five P-T curves have been prepared which are valid through 28 EFPY: heatup and cooldown for non-critical operations; heatup and cooldown for critical operations; and non-critical leakage/hydrotest. In addition, leak/hydro test curves have been prepared at exposures of 20 EFPY and 24 EFPY. These curves have been developed to minimize outage time associated with the slow heatup rate to the test temperature which is inherent in a BWR plant.

4.8 Chapter 4 References

[4-1] U.S. NRC Regulatory Guide 1.99, "Radiation Embrittlement of Reactor Vessel Materials," Revision 2, May 1988.

[4-2] Generic Letter 92-01 and RPV Integrity Assessment, NRC/Industry Workshop on RPV Integrity Issues, February 12, 1998

[4-3] Edwards, A. L., "TRUMP: A Computer Program for Transient and Steady-State Temperature Distributions in Multidimensional Systems," Lawrence Radiation Laboratory, Livermore, Report UCRL-14754, Revision 2 (1968).

[4-4] PT Curve™ Version 1.0, MPM Technologies, Inc. Code Manual, Document No. MPM-196201, March 25, 1996

[4-5] Letter from Annett, M.G. to Manahan, M.P., "Instrument Uncertainty for PT Curves", M97-080, December 18, 1997

[4-6] Manahan, M. P., Y. Soong, "Response to NRC Generic Letter 92-01 for Nine Mile Point Unit 1, MPM-GL-692713, June, 1992

Table 4-1 Surveillance Data Credibility Assessment for Plate G-8-1

Capsule Identification	Fluence (n/cm^2)	Fluence Factor (FF)	Measured ΔRT_{NDT} (F)	Predicted ΔRT_{NDT} (Surveillance CF) (F)	Measured ΔRT_{NDT} Minus Predicted ΔRT_{NDT} (F)
30°	3.60×10^{17}	0.244	54.0	53.98	0.02
210°	1.00×10^{18}	0.417	77.7	92.24	-14.54
300°	4.78×10^{17}	0.286	84.4	63.20	21.19

Table 4-2 RG1.99(2) Table CF Applicability Analysis for Plate G-8-1

Capsule Identification	Fluence (n/cm^2)	Fluence Factor (FF)	Measured ΔRT_{NDT} (F)	Predicted ΔRT_{NDT} + 34 F (RG1.99(2) Table CF) (F)	Measured ΔRT_{NDT} Minus Predicted ΔRT_{NDT} + 34 F (F)
30°	3.60×10^{17}	0.244	54.0	71.56	-17.56
210°	1.00×10^{18}	0.417	77.7	98.18	-20.48
300°	4.78×10^{17}	0.286	84.4	77.98	6.42

Table 4-3 Summary of Beltline Initial RT_{NDT} Data [4-6]

Material	RT_{NDT} (TL) (°F)
plate G-8-3/G-8-4	-3
plate G-8-1	36
plate G-307-3	28
plate G-307-4	40
plate G-307-10	20
weld W5214/5G13F	-50
weld 86054B/4E5F	-50
weld 1248/4K13F	-50
weld 1248/4M2F	-50

Table 4-4 Analysis of NMP-1 Beltline Materials at 28 EFPY to Identify Limiting ART

Material ID	1/4 T Fluence (n/cm^2)	RG1.99 Fluence Factor (FF)	Cu Content (wt %)	Ni Content (wt %)	RG 1.99 Chemistry Factor (CF) (F)	RG 1.99 Source of CF	Initial RT_{NDT} (TL) (F)	ΔRT_{NDT} (F)	Margin (F)	ART (F)
Plate G-307-4/5	1.76×10^{18}	0.539	0.27	0.53	173.85	Table	40	93.7	34	167.7
Plate G-307-3	1.76×10^{18}	0.539	0.20	0.48	134.60	Table	28	72.6	34	134.6
Plate G-307-10	1.76×10^{18}	0.539	0.22	0.51	148.85	Table	20	80.3	34	134.3
Plate G-8-1 [a]	9.60×10^{17}	0.409	0.23	0.51	221.26	Surveillance Data	36	90.5	34	160.5
Plate G-8-3/4 [a]	9.60×10^{17}	0.409	0.18	0.56	130.20	Table	-3	53.3	34	84.3
Weld Seam 2-564 A/C [b]	1.76×10^{18}	0.539	0.22	0.20	112.0	Table	-50	60.4	56	66.4
Weld Seam 2-564 D/F [b]	1.76×10^{18}	0.539	0.22	0.20	112.0	Table	-50	60.4	56	66.4
Weld Seam 3-564 [b]	1.76×10^{18}	0.539	0.22	0.20	112.0	Table	-50	60.4	56	66.4

[a]The fluence to the lower shell course plates is lower than that of the upper shell plates because the axial flux peak is above the core midplane.
[b]The Cu and Ni content of the beltline welds is from [4-6], and the resulting CF value is bounding for these materials.

Table 4-5 Summary Of Nine Mile Point Unit 1 Parameters Used In P-T Curve Calculations

Parameter	Value	Reference
vessel base metal inner radius	106.5 in	FSAR Table V-1
vessel base metal outer radius	113.625 in	FSAR Table V-1
wall thickness (base metal)	7 1/8 in	FSAR Table V-1
vessel clad thickness	5/32 in	FSAR Table V-1
peak wall ID surface fast flux (E > 1 Mev)	3.05×10^9 n/cm^2/sec	This Report
RT_{NDT} for limiting material	40°F	Reference [4-6]
pre-operational hydrotest	1800 psig	Technical Specification Bases for 2.2.1
RT_{NDT} of non-beltline materials	40°F	Technical Specification Bases for 3.2.2 and 4.2.2
system operating pressure	1030 psig	Technical Specification Bases for 2.2.1
yield strength of limiting material	69.4 ksi	Reference [4-6]
temperature instrument error	4.0°F (leak/hydro) 12.2°F (heatup/cooldown)	Reference [4-5]
pressure instrument error	10.0 psig (leak/hydro) 52.2 psig (heatup/cooldown)	References [4-5]
standard deviation for the initial RT_{NDT}	0°F	Reference [4-6]
RG1.99(2) σ_Δ	17°F	Reference [4-1]

Table 4-6 **Minimum Beltline Downcomer Water Temperature for Pressurization During Heat-Up (Core Not Critical) (Heating Rate ≤ 100°F/Hr) For Up To 28 Effective Full Power Years of Operation**

REACTOR PRESSURE (psig) IN TOP DOME	REACTOR VESSEL BELTLINE DOWNCOMER WATER TEMPERATURE (F)[a]
197	100
197	110
197	120
197	130
199	140
205	150
213	160
225	170
239	180
257	190
279	200
304	210
334	220
369	230
410	240
458	250
513	260
577	270
651	280
737	290
835	300
949	310
1079	320

[a] Reactor Vessel Beltline Downcomer Water Temperature is Measured at Recirculation Loop Suction Instrument Uncertainties Have Been Included in this Table

Table 4-7 Minimum Beltline Downcomer Water Temperature For Pressurization During Cooldown (Core Not Critical) (Cooling Rate ≤ 100°F/Hr) For Up To 28 Effective Full Power Years of Operation

REACTOR PRESSURE (psig) IN TOP DOME	REACTOR VESSEL BELTLINE DOWNCOMER WATER TEMPERATURE (F)[a]
160	100
171	110
184	120
199	130
216	140
235	150
258	160
284	170
315	180
350	190
391	200
438	210
493	220
556	230
630	240
708	250
786	260
866	270
957	280
1062	290

[a] Reactor Vessel Beltline Downcomer Water Temperature is Measured at Recirculation Loop Suction
Instrument Uncertainties Have Been Included in this Table

Table 4-8 **Minimum Beltline Downcomer Water Temperature For Pressurization During Heatup (Core Critical) (Heating Rate ≤ 100°F/Hr) For Up To 28 Effective Full Power Years of Operation**

REACTOR PRESSURE (psig) IN TOP DOME	REACTOR VESSEL BELTLINE DOWNCOMER WATER TEMPERATURE (F)[b]
197	100
197	110
197	120
197	130
197	140
197	150
197	160
197	170
199	180
205	190
213	200
225	210
239	220
257	230
279	240
304	250
334	260
360	268
360	270
360	277
402	278[a]
410	280
458	290
513	300
577	310
651	320
737	330
835	340
949	350
1079	360

[a] Water Level Must be in Range for Power Operation if Core is Critical Below 278°F

[b] Reactor Vessel Beltline Downcomer Water Temperature is Measured at Recirculation Loop Suction Instrument Uncertainties Have Been Included in this Table

Table 4-9 **Minimum Beltline Downcomer Water Temperature For Pressurization During Cooldown (Core Critical) (Cooling Rate ≤ 100°F/Hr) For Up To 28 Effective Full Power Years of Operation**

REACTOR PRESSURE (psig) IN TOP DOME	REACTOR VESSEL BELTLINE DOWNCOMER WATER TEMPERATURE (F)[b]
130	100
136	110
143	120
151	130
160	140
171	150
184	160
199	170
216	180
235	190
258	200
284	210
315	220
350	230
360	233
360	240
360	250
360	259
493	260[a]
556	270
630	280
708	290
786	300
866	310
957	320
1062	330

[a] Water Level Must be in Range for Power Operation if Core is Critical Below 260°F

[b] Reactor Vessel Beltline Downcomer Water Temperature is Measured at Recirculation Loop Suction Instrument Uncertainties Have Been Included in this Table

Table 4-10 Minimum Beltline Downcomer Water Temperature For Pressurization During In-Service Hydrostatic Testing and Leak Testing (Core Not Critical) For Up To 28 Effective Full Power Years of Operation

REACTOR PRESSURE (psig) IN TOP DOME	REACTOR VESSEL BELTLINE DOWNCOMER WATER TEMPERATURE (F)[a]
360	100
360	110
360	120
360	130
569	140
590	150
614	160
642	170
675	180
712	190
755	200
805	210
862	220
929	230
1005	240
1032	243
1093	250
1195	260

[a] Reactor Vessel Beltline Downcomer Water Temperature is Measured at Recirculation Loop Suction Instrument Uncertainties Have Been Included in this Table

Table 4-11 **Minimum Beltline Downcomer Water Temperature For Pressurization During In-Service Hydrostatic Testing and Leak Testing (Core Not Critical) For Up To 20 Effective Full Power Years of Operation**

REACTOR PRESSURE (psig) IN TOP DOME	REACTOR VESSEL BELTLINE DOWNCOMER WATER TEMPERATURE (F)[a]
360	100
360	110
360	120
360	130
597	140
622	150
652	160
685	170
724	180
769	190
821	200
881	210
951	220
1031	230
1123	240
1229	250

[a] Reactor Vessel Beltline Downcomer Water Temperature is Measured at Recirculation Loop Suction
Instrument Uncertainties Have Been Included in this Table

Table 4-12 **Minimum Beltline Downcomer Water Temperature For Pressurization During In-Service Hydrostatic Testing and Leak Testing (Core Not Critical) For Up To 24 Effective Full Power Years of Operation**

REACTOR PRESSURE (psig) IN TOP DOME	REACTOR VESSEL BELTLINE DOWNCOMER WATER TEMPERATURE (F)[a]
360	100
360	110
360	120
360	130
582	140
604	150
631	160
661	170
697	180
737	190
785	200
839	210
902	220
974	230
1033	237
1058	240
1154	250

[a] Reactor Vessel Beltline Downcomer Water Temperature is Measured at Recirculation Loop Suction
Instrument Uncertainties Have Been Included in this Table

HEATUP - CORE NOT CRITICAL

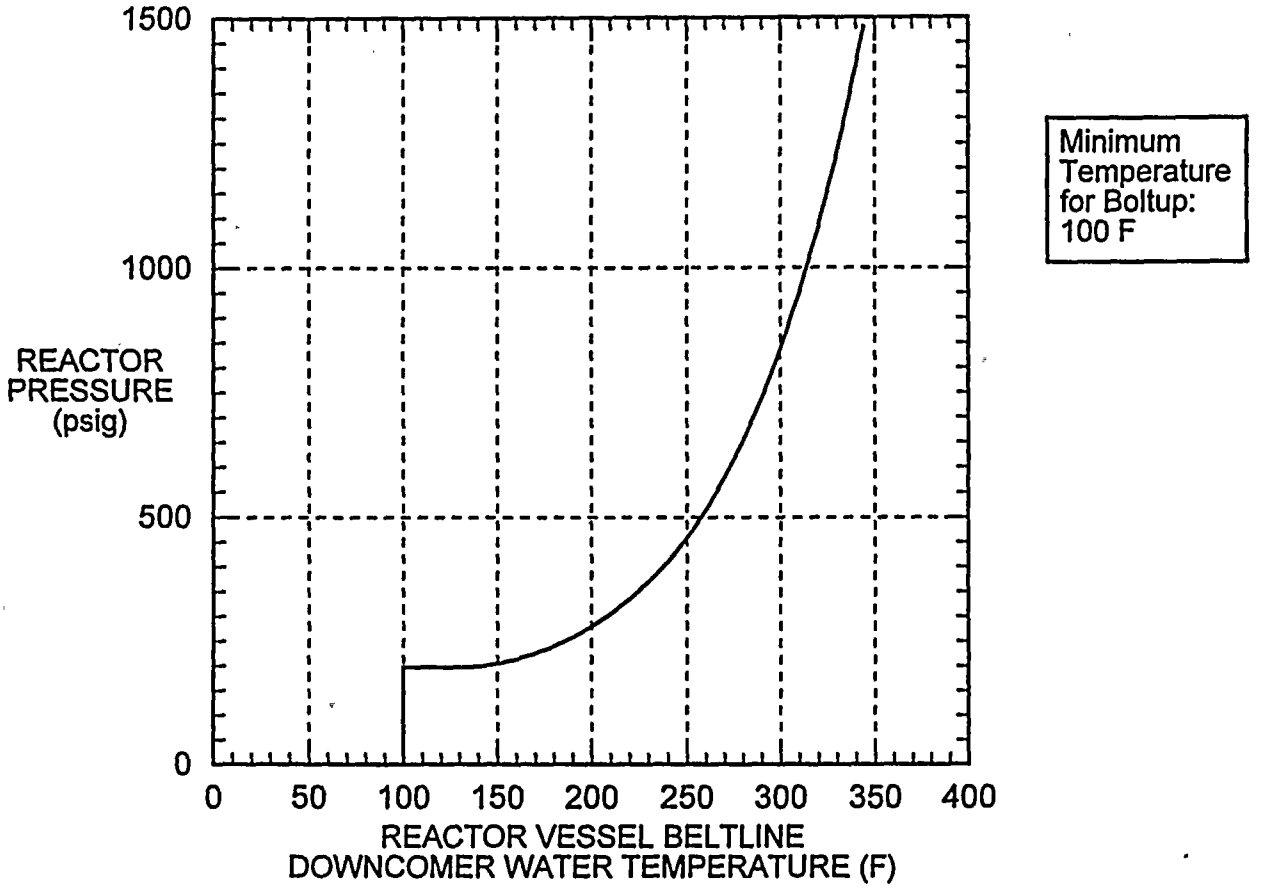

Instrument Uncertainties Have Been Included in this Figure

Figure 4-1 **Minimum Beltline Downcomer Water Temperature for Pressurization During Heatup (Core Not Critical) (Heating Rate ≤ 100°F/Hr) For Up To 28 Effective Full Power Years of Operation**

COOLDOWN - CORE NOT CRITICAL

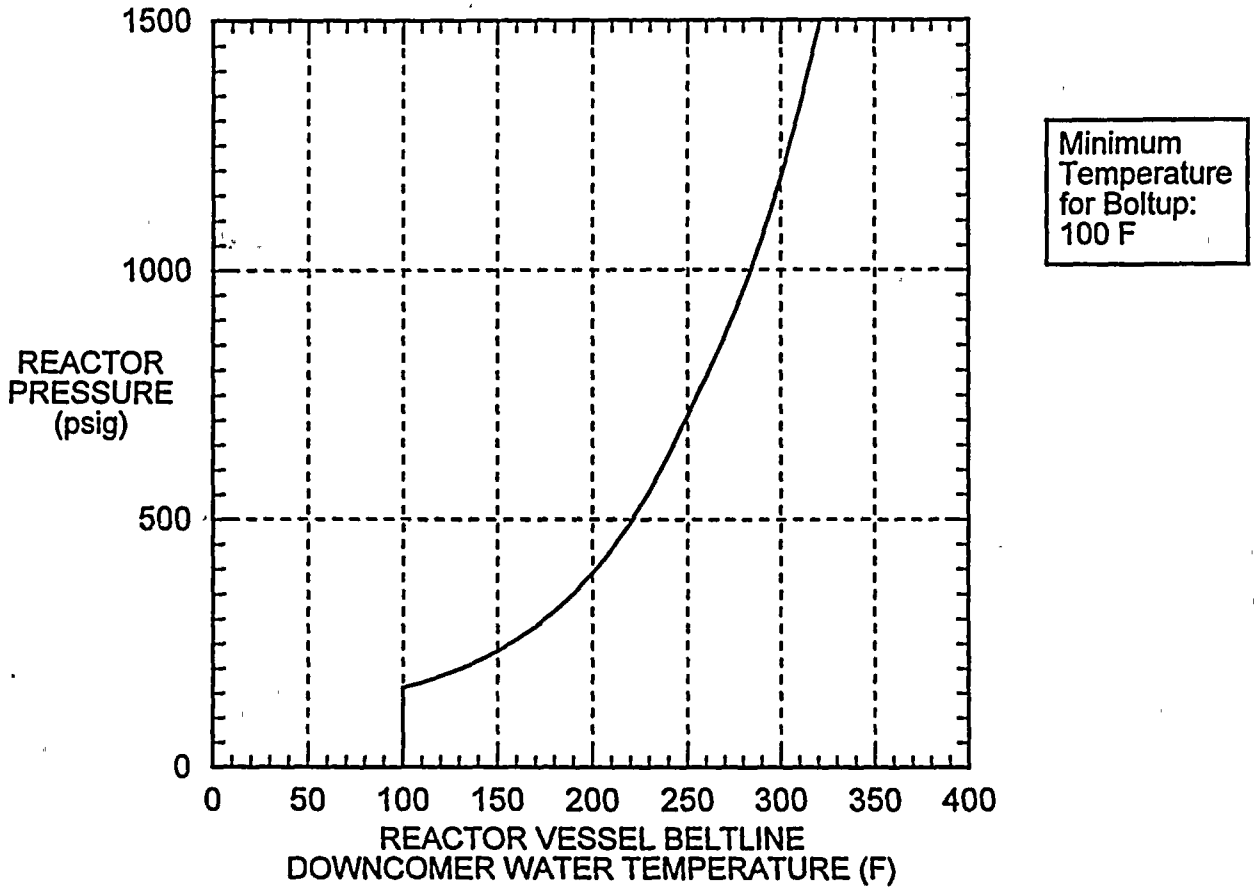

Instrument Uncertainties Have Been Included in this Figure

Figure 4-2 **Minimum Beltline Downcomer Water Temperature for Pressurization During Cooldown (Core Not Critical) (Cooling Rate ≤ 100°F/Hr) For Up To 28 Effective Full Power Years of Operation**

HEATUP - CORE CRITICAL

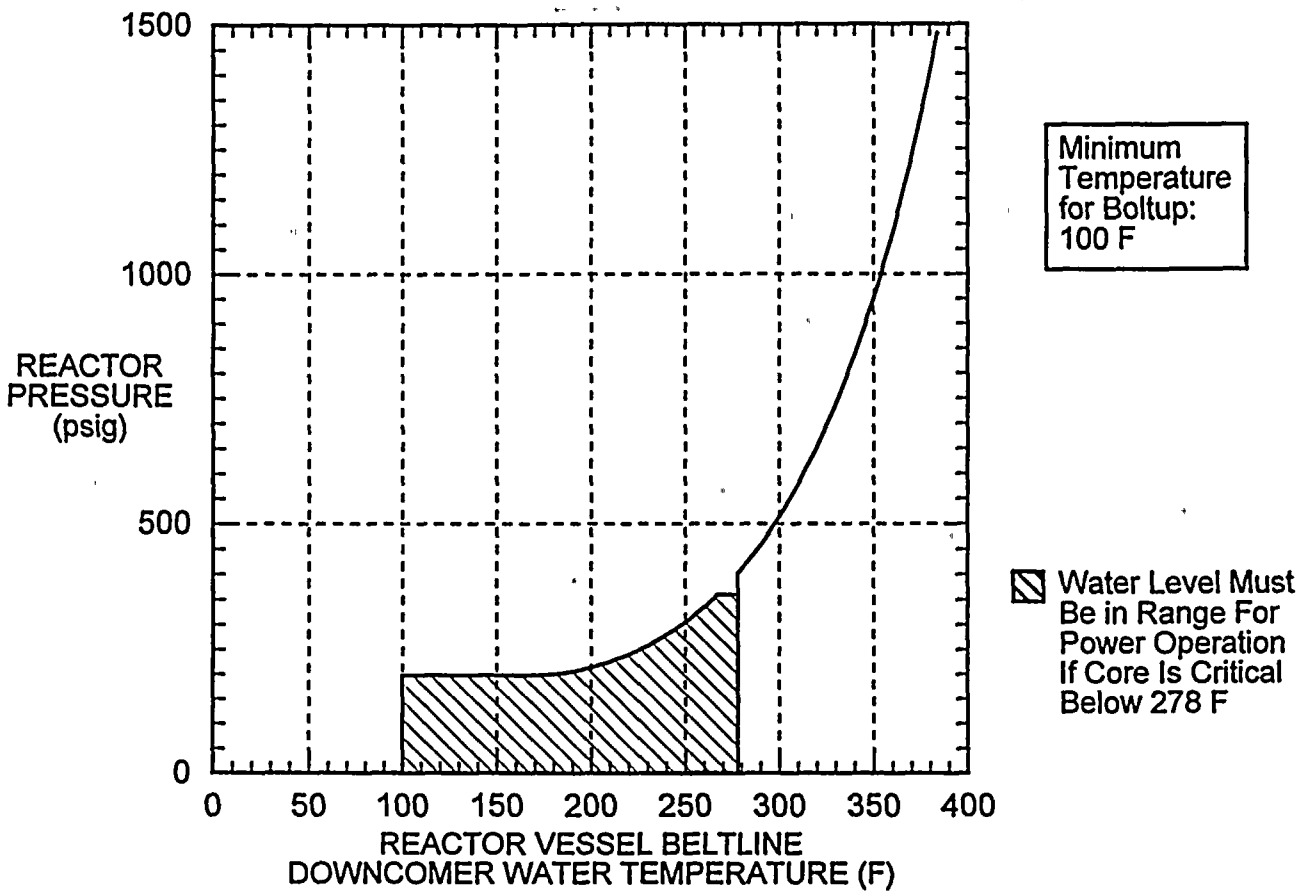

Instrument Uncertainties Have Been Included in this Figure

Figure 4-3 **Minimum Beltline Downcomer Water Temperature for Pressurization During Heatup (Core Critical) (Heating Rate ≤ 100°F/Hr) For Up To 28 Effective Full Power Years of Operation**

COOLDOWN - CORE CRITICAL

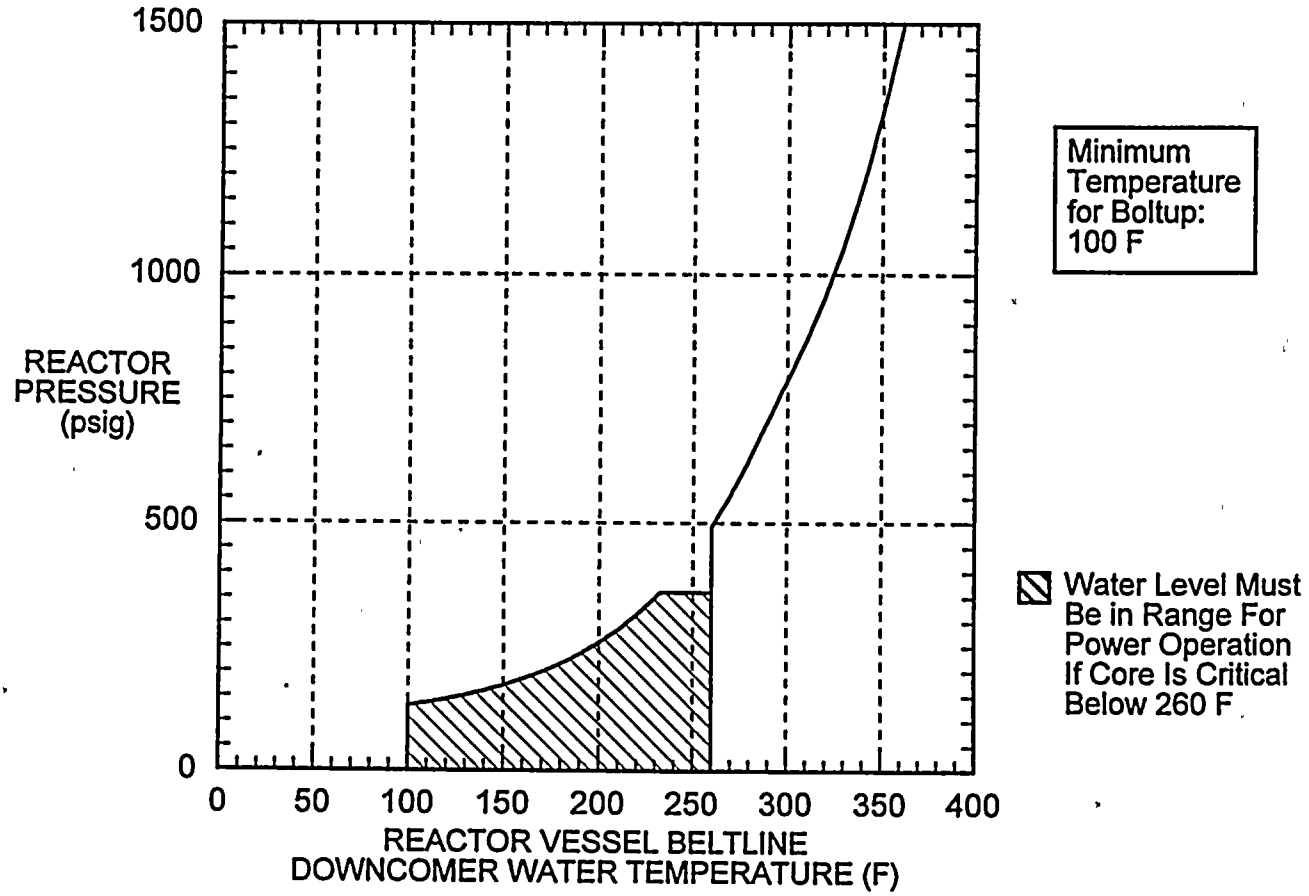

Instrument Uncertainties Have Been Included in this Figure

Figure 4-4 **Minimum Beltline Downcomer Water Temperature for Pressurization During Cooldown (Core Critical) (Cooling Rate ≤ 100°F/Hr) For Up To 28 Effective Full Power Years of Operation**

LEAK/HYDRO TEST - CORE NOT CRITICAL

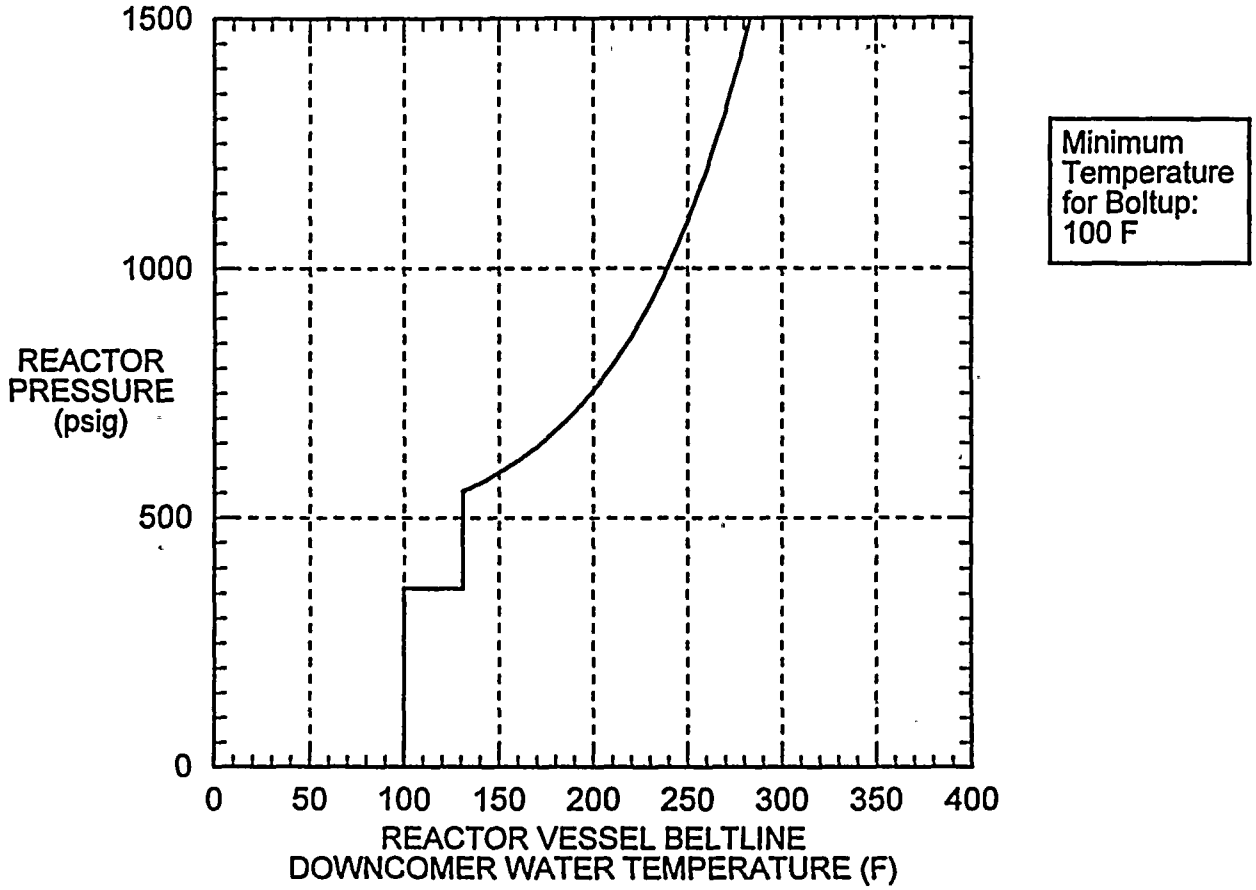

Instrument Uncertainties Have Been Included in this Figure

Figure 4-5 Minimum Beltline Downcomer Water Temperature for Pressurization During In-Service Hydrostatic Testing and Leak Testing (Core Not Critical) For Up To 28 Effective Full Power Years of Operation

LEAK/HYDRO TEST - CORE NOT CRITICAL

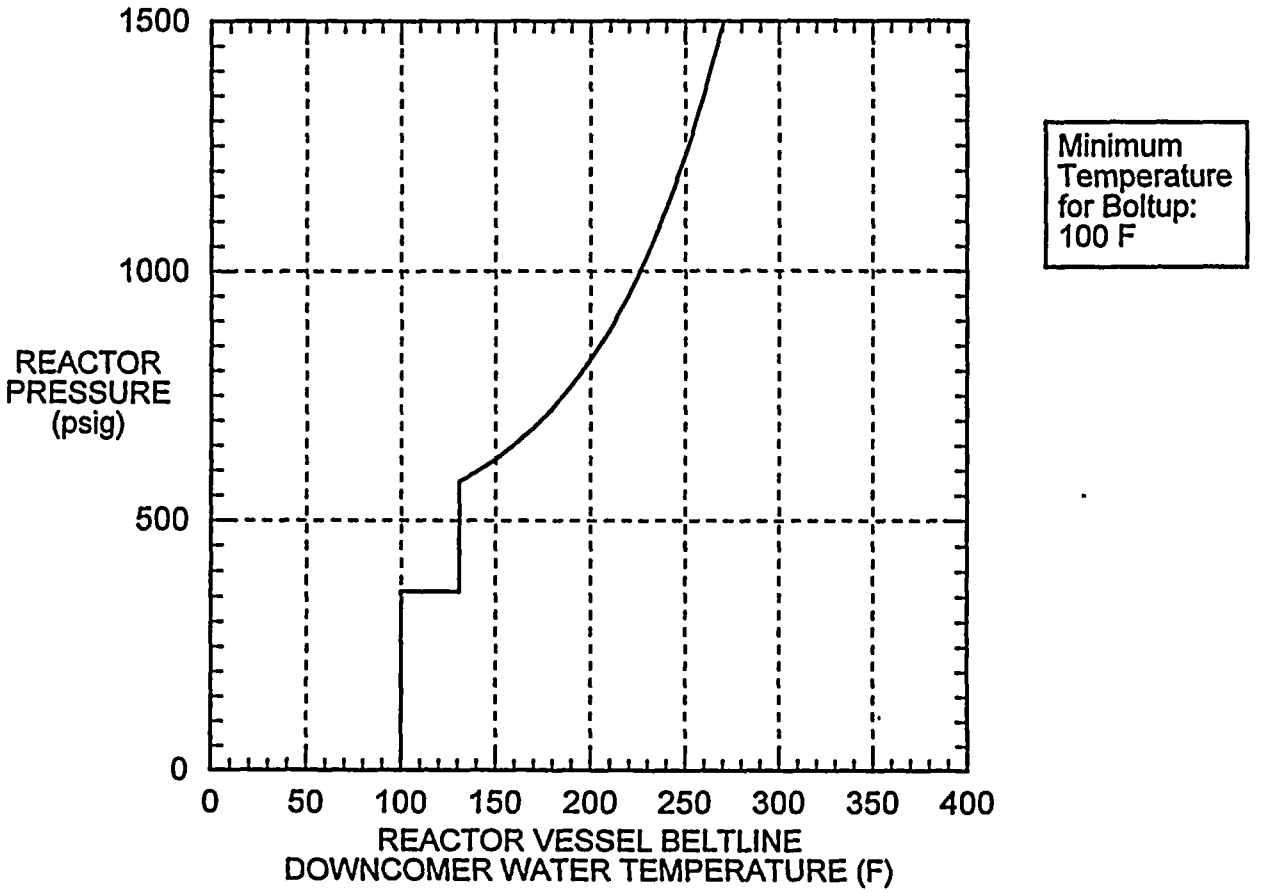

Instrument Uncertainties Have Been Included in this Figure

Figure 4-6 Minimum Beltline Downcomer Water Temperature for Pressurization During In-Service Hydrostatic Testing and Leak Testing (Core Not Critical) For Up To 20 Effective Full Power Years of Operation

LEAK/HYDRO TEST - CORE NOT CRITICAL

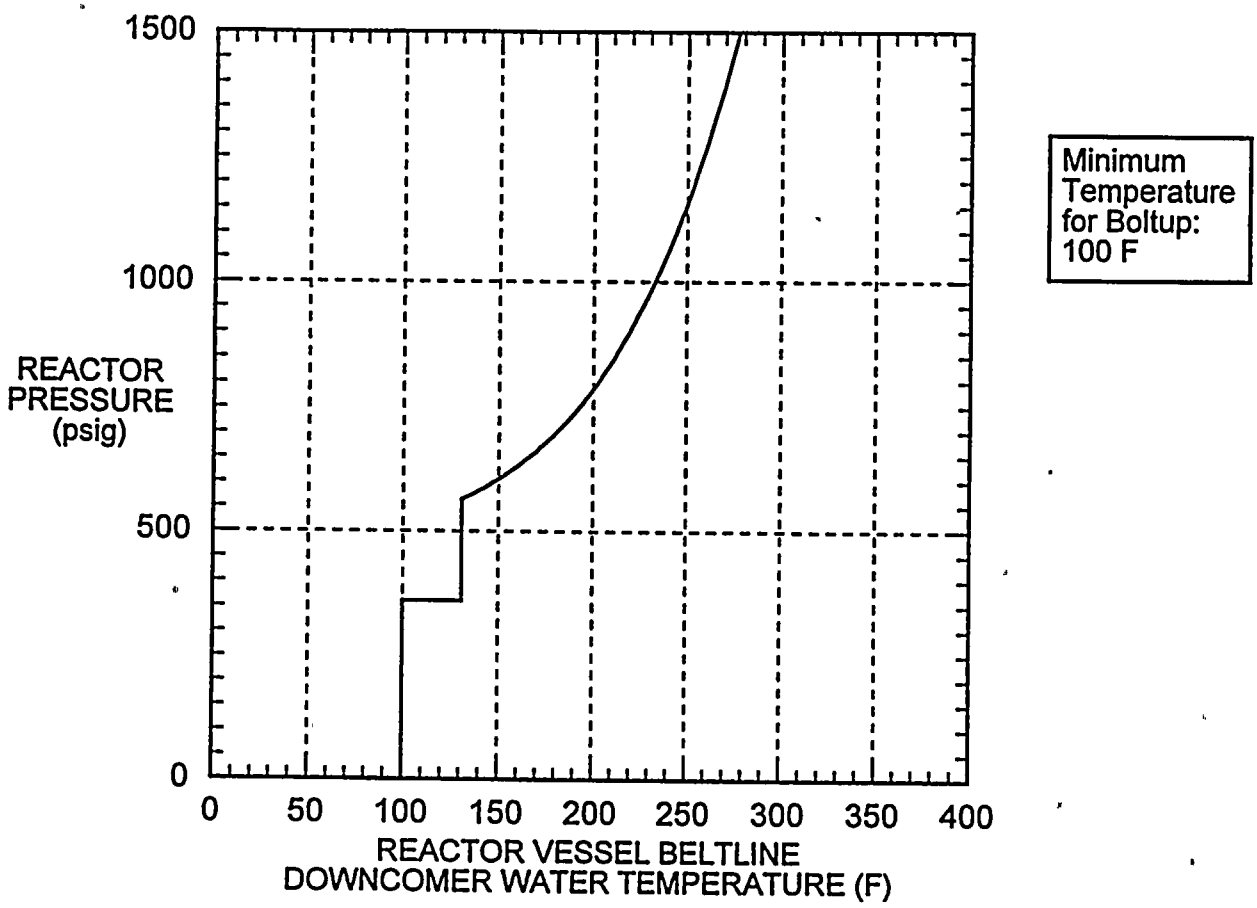

Instrument Uncertainties Have Been Included in this Figure

Figure 4-7 Minimum Beltline Downcomer Water Temperature for Pressurization During In-Service Hydrostatic Testing and Leak Testing (Core Not Critical) For Up To 24 Effective Full Power Years of Operation

5.0 Summary

P-T operating curves for NMP-1 have been calculated for up to 28 EFPY of operation. These new P-T curves satisfy the requirements of 10CFR50, Appendix G. Operation of NMP-1 in accordance with the revised P-T operating limits will preclude brittle fracture of the RPV materials. Safety margins for brittle fracture are in accordance with those specified in 10CFR50, Appendix G and Appendix G to Section III of the ASME Code. Therefore, the revised P-T limits do not involve a significant increase in the probability or consequences of an accident previously evaluated, do not introduce the possibility of a new or different kind of accident, and do not significantly reduce existing margins of safety.

The current P-T curves, which are valid up to 18 EFPY, require a minimum temperature for leak testing at 1030 psig of 216 F. The revised minimum leak test temperature for up to 28 EFPY is 243 F. In order to minimize outage time, minimum leak test temperatures were calculated for exposures of 20 EFPY and 24 EFPY. The minimum leak test temperatures at these two additional exposures are: 20 EFPY - 230 F; and 24 EFPY - 237 F.

6.0 Nomenclature

ART	adjusted reference temperature
ASME	American Society of Mechanical Engineers
ASTM	American Society for Testing and Materials
BWR	boiling water reactor
CFR	Code of Federal Regulations
EFPY	effective full power years
F, °F	degrees Fahrenheit
EOL	end-of-license
FSAR	Final Safety Analysis Report
ID	inner diameter
IG	intergranular
K_{IR}	ASME reference stress intensity factor curve
NMP-1	Nine Mile Point Unit 1
NMPC	Niagara Mohawk Power Corporation
NRC	Nuclear Regulatory Commission
P_o	operating pressure
P-T	pressure-temperature
PR-EDB	Power Reactor Embrittlement Data Base
PTCurve	MPM Technologies, Inc. allowable RPV pressure-temperature code package
RG1.99(2)	Regulatory Guide 1.99 (Revision 2)
RPV	reactor pressure vessel
ΔRT_{NDT}	neutron induced shift in RT_{NDT}
RT_{NDT}	nil-ductility reference temperature
σ_I	standard deviation for the initial RT_{NDT}
σ_Δ	standard deviation for ΔRT_{NDT}
σ_y	material yield strength
T	vessel wall thickness
ΔT_{30}	Charpy curve shift indexed at the 30 ft-lb
T_c	downcomer coolant temperature
T_{CRIT}	minimum temperature for plant operation using nuclear heat with the core critical
TRPC	thermophysical properties of matter data series
TRUMP	Livermore multi-dimensional transient temperature distribution code
ΔUSE	drop in the upper shelf energy